

NORSAR

ROYAL NORWEGIAN COUNCIL FOR SCIENTIFIC AND INDUSTRIAL RESEARCH

Norsar Technical Report No. 2/81

TRAVEL TIME AND WAVEFRONT CURVATURE CALCULATIONS IN INHOMOGENEOUS LAYERED MEDIA WITH CURVED INTERFACES

by
H. Gjøystdal, J. E. Reinhardsen and B. Ursin

Tilhører NORSAR

October 1981

NORSAR Contribution No. 306



Society of Exploration Geophysicists

Box 3098

Tulsa, Oklahoma 74101

Preprint subject to later revision,
for information of delegates to the SEG Annual Meeting only.

TRAVEL TIME AND WAVEFRONT CURVATURE CALCULATIONS IN
INHOMOGENEOUS LAYERED MEDIA WITH CURVED INTERFACES

by

H. Gjøystdal*, J.E. Reinhardsen* and B. Ursin**

Publication rights are reserved. This paper is to be presented at the 51st Annual International Meeting of the Society of Exploration Geophysicists in Los Angeles, California. GEOPHYSICS has first claim on this paper for publication. Publication elsewhere is hereby restricted to the author's abstract or to an abstract of not more than 300 words, without illustration, unless the paper is specifically released by the Editor of GEOPHYSICS or the Executive Director on his behalf. Such abstract should contain appropriate conspicuous acknowledgement.

Discussion of this paper is invited immediately after its presentation. Written discussions will be considered for publication in GEOPHYSICS should the paper be accepted for publication

* Address: NTNF/NORSAR, Post Box 51, N-2007 Kjeller, Norway

** Address: SINTEF, Division of Petroleum Engineering, N-7034 Trondheim-NTH, Norway

ABSTRACT

The seismic rays and wavefront curvature are determined by solving a system of non-linear ordinary differential equations. For media with constant velocity and for media with constant velocity gradient simplified solutions exist. In a general inhomogeneous medium these equations must be solved by numerical approximations. The ray-tracing and wavefront curvature integration is then performed by a modified divided difference form of the Adams PECE (Predict - Evaluate - Correct - Evaluate) formulas and local extrapolation. The estimation of the predicted value is done by the Adams-Bashforth formula, while the correction is obtained by use of the Adams-Moulton formula.

The interfaces between the layers are represented by bicubic splines. The change in ray direction and wavefront curvature at the interfaces are computed using standard formulas.

For three-dimensional media two quadratic travel time approximations have been proposed. Both are based on a Taylor series expansion with reference to a ray from a reference source point to a reference receiver point. The first approximation corresponds to expanding the square of the travel time in a Taylor series and taking the square root of the result. The second approximation corresponds to expanding the travel time in a Taylor series. Numerical computations for different three-dimensional models indicate that the first approximation is, in most cases, the most accurate.

The travel time approximation may be expressed in source-receiver coordinates or in midpoint-half offset coordinates. Simplified expressions are obtained when the reference source and receiver coincide, giving zero offset approximations for which the reference ray is a normal-incidence ray. These simplified travel time approximations may be used in a three-dimensional seismic velocity analysis. Instead of estimating the stacking velocity one must estimate three elements in a 2×2 symmetric matrix. The accuracy and range of validity of the simplified travel time approximations are investigated for different three-dimensional models.

INTRODUCTION

Travel time and wavefront curvature are useful parameters in seismic modeling and inversion (Taner et al, 1970; Gjøystdal and Ursin, 1981). It is well known that the seismic rays and wavefront curvature can be determined by solving a system of non-linear ordinary differential equations (Shah, 1973; Popov and Pšenčík, 1978A,B; Hubral, 1979; Červený and Hron, 1980). We shall describe numerical procedures for solving these equations for general 3-D inhomogeneous media.

The numerical algorithms will be used to investigate the accuracy of two proposed travel time approximations (Ursin, 1981C). Both approximations are based on Taylor series expansions with respect to a ray from a reference source point to a reference receiver point. For the zero-offset case the parameters defining the travel time approximations can be computed using wavefront curvature calculations. In this case we shall consider a number of different 3-D models, and compare the travel time errors of the two approximations mentioned. We shall also investigate the accuracy of different methods for velocity analysis in these models.

For a three-dimensional medium consisting of homogeneous layers with plane dipping interfaces the travel time approximation will be simplified. The derived travel time approximation is exact for a reflection from a plane dipping interface in a homogeneous medium.

RAY-TRACING AND WAVEFRONT CURVATURE EQUATIONS

Let $x = (x_1, x_2, x_3)^T$ be coordinates in a fixed coordinate system with the x_3 -axis vertically downward (all vectors are considered to be column vectors and superscript T denotes transposition). We consider a subsurface model consisting of inhomogeneous layers separated by curved interfaces. Shah (1973) has given a method for computing the ray from a source point to a receiver point for a specified type of ray. The ray location vector $x(\sigma)$ and the unit vector tangent to the ray, $m(\sigma)$, satisfy the following set of differential equations

$$\frac{dx}{d\sigma} = m \quad (1a)$$

$$\frac{dm}{d\sigma} = -\frac{1}{v} \frac{dv}{d\sigma} m - \frac{1}{v} \nabla v \quad (1b)$$

where σ denotes arclength along the ray, v is the velocity of wave propagation, and the velocity gradient is given by

$$\nabla v = \left(\frac{\partial v}{\partial x_1}, \frac{\partial v}{\partial x_2}, \frac{\partial v}{\partial x_3} \right)^T$$

We note that

$$\frac{dv}{d\sigma} = m^T \nabla v \quad (2)$$

The initial conditions $x(\sigma_0)$ and $m(\sigma_0)$ must be specified at some suitable starting point. The travel time is given by

$$t(\sigma) = t(\sigma_0) + \int_{\sigma_0}^{\sigma} \frac{d\xi}{v(\xi)} \quad (3)$$

The ray is reflected or refracted at an interface $f(x) = 0$ between two inhomogeneous layers. The surface normal at the point of intersection with the ray is

$$n_3 = \nabla f / \|\nabla f\| \quad (4)$$

pointing out from the surface into the medium containing the refracted ray as shown in Fig. 1. In equation (4) we have used the norm $\|x\| = (x^T x)^{1/2}$.

The incident and the refracted ray are shown in Fig. 1 where v_I is the velocity of the incident wave, m_I is the direction of the incident ray and α_I is the angle between the interface normal and the incident ray. The corresponding quantities for the refracted ray are denoted by v_R , m_R and α_R . At the interface we use the equation

$$\frac{m_R}{v_R} = \frac{m_I}{v_I} + \left(\frac{\cos \alpha_R}{v_R} - \frac{\cos \alpha_I}{v_I} \right) n_3 \quad (5)$$

We shall use a ray-centered coordinate system which is moving with the wavefront along the ray (Popov and Pšenčík, 1978A&B; Hubral, 1979; Červený and Hron, 1980). The basis of this coordinate system is formed by the mutually orthogonal vectors e_1 , e_2 and m , and the related coordinates are denoted by (u_1, u_2, z) . The main advantage of using this new coordinate system is that the wavefront curvature calculations are much simplified. In dynamic ray-tracing calculations the differential equations for P- and S-waves decouple when expressed in this coordinate system (Červený and Hron, 1980). The same orthogonal coordinate system has also been used in solving electromagnetic wave propagation problems (Tang, 1970; Lewin, Chang and Kuester, 1977).

Hubral (1979) has shown that the wavefront curvature matrix A satisfies the symmetric Riccati differential equation

$$v \frac{dA}{d\sigma} - \frac{dv}{d\sigma} A + vA^2 + C = 0 \quad (6)$$

where the 2x2 symmetric matrix C has elements

$$C_{ij} = \frac{\partial^2 v}{\partial u_i \partial u_j}$$

which can be found from (see Popov and Pěněčik, 1978b, equation (2.19))

$$C = \begin{bmatrix} e_1^T \\ e_2^T \end{bmatrix} V [e_1, e_2] \quad (7)$$

where V is a 3x3 symmetric matrix with elements

$$V_{ij} = \frac{\partial^2 v}{\partial x_i \partial x_j}$$

In some cases the computations are simplified if we consider the radius of curvature matrix $R = A^{-1}$ or if we consider the matrix $G = vR = vA^{-1}$. Equation (6) then becomes

$$\frac{dG}{d\sigma} - vI - v^{-2} GCG = 0 \quad (8)$$

(This is equation (73) in Červený and Hron (1980).)

In order to compute the transformation of the wavefront curvature matrix at an interface between two inhomogeneous media, we need to introduce a new coordinate system defined by the orthogonal vectors e_{I1} , e_{I2} and m_I , where $m_I = m(\sigma_I)$ and e_{I1} is in the plane of incidence defined by the interface normal n_3 and the ray tangent $m(\sigma_I)$. Let (u_{I1}, u_{I2}, z_I) be the coordinates of this new coordinate system which is obtained from the (e_1, e_2, m) system by rotating the latter an angle δ around the m -axis. Then

$$u = \begin{bmatrix} \cos \delta & \sin \delta \\ -\sin \delta & \cos \delta \end{bmatrix} u_I = Du_I \quad (9)$$

and the wavefront curvature matrix in the new system is

$$A_I = D^T A(\sigma_I) D \quad (10)$$

For the refracted ray we use the coordinate system defined by the vectors (e_{R1}, e_{R2}, m_R) such that $m_R = m(\sigma_R)$ is the direction of the outgoing ray, e_{R1} is in the plane of incidence and $e_{R2} = e_{I2}$. We let u_{R1} , u_{R2} and z_R be the coordinates in this system, and the wavefront curvature matrix is denoted by A_R . The wavefront curvature calculations are restarted with $A(\sigma_R) = A_R$ and $e_1 = e_{R1}$.

Finally we need the coordinate system shown in Fig. 1 defined by the vectors (η_1, η_2, η_3) where η_3 is the interface normal, η_1 is in the plane of incidence and $\eta_2 = e_{I2} = e_{R2}$. We let η_1 , η_2 and η_3 be the coordinates of this system. The interface is approximated near the point of intersection with the ray by the quadratic expression

$$\eta_3 + \frac{1}{2} [\eta_1, \eta_2] F \begin{matrix} \eta_1 \\ \eta_2 \end{matrix} = 0 \quad (11)$$

where F is a 2x2 symmetric matrix with elements

$$F_{ij} = \frac{\partial^2 f}{\partial \eta_i \partial \eta_j}$$

By expanding equation (5) in a Taylor series in the η -coordinate system and assuming that all terms in the direction of the interface normal are small, it is shown in Ursin (1981B) that the wavefront curvature matrix of the refracted wave is given by

$$A_R = v_R S_R^{-1} \left\{ \frac{1}{v_I} S_I A_I S_I + \left(\frac{\cos \alpha_R}{v_R} - \frac{\cos \alpha_I}{v_I} \right) F \right.$$

$$+ \frac{\sin \alpha_R}{v_R^2} \left[\begin{array}{l} 2 \cos \alpha_R \frac{\partial v_R}{\partial u_{R1}} + \sin \alpha_R \frac{dv_R}{d\sigma_R}, \frac{\partial v_R}{\partial u_{R2}} \\ \frac{\partial v_R}{\partial u_{R2}}, 0 \end{array} \right]$$

(12)

$$- \frac{\sin \alpha_I}{v_I^2} \left[\begin{array}{l} 2 \cos \alpha_I \frac{\partial v_I}{\partial u_{I1}} + \sin \alpha_I \frac{dv_I}{d\sigma_I}, \frac{\partial v_I}{\partial u_{I2}} \\ \frac{\partial v_I}{\partial u_{I2}}, 0 \end{array} \right] \} S_R^{-1}$$

where

$$S_R = \begin{bmatrix} \cos \alpha_R & 0 \\ 0 & 1 \end{bmatrix} \tag{13}$$

and S_I is similarly defined. This formula is also given in Hubral (1980) and in Červený and Hron (1980), where it is obtained by use of phase matching.

For a reflected wave of the same type as the incident wave ($v_R = v_I$) the wavefront curvature matrix is given by

$$A_R = EA_1 E - ES_I^{-1} \left\{ 2\cos\alpha_I F + \frac{\sin 2\alpha_I}{v_I} \begin{bmatrix} \frac{\partial v_I}{\partial u_{I1}} + \frac{\partial v_I}{\partial u_{R1}} + \sin\alpha_I \frac{\partial v_I}{\partial \eta_3}, 0 \\ 0, 0 \end{bmatrix} \right\} S_I^{-1} E \quad (14)$$

where

$$E = \begin{bmatrix} -1 & 0 \\ 0 & 1 \end{bmatrix} \quad (15)$$

SOLUTIONS OF THE EQUATIONS

Homogeneous medium

In a homogeneous medium the ray paths are straight lines given by

$$x(\sigma) = x(\sigma_0) + m(\sigma_0)(\sigma - \sigma_0) \quad (16)$$

The radius of curvature matrix is computed from (Hubral, 1979)

$$R(\sigma) = R(\sigma_0) + I(\sigma - \sigma_0) \quad (17)$$

where I is a 2x2 identity matrix.

Medium with constant velocity gradient

The equations for ray-tracing and wavefront curvature calculations can be simplified in a medium with constant velocity gradient (Hubral, 1980; Ursin, 1981A). The velocity function is

$$v(x) = v(0) + \nabla v^T x \quad (18)$$

where the velocity gradient ∇v is constant. From equations (1b) and (2) we see that m , and therefore the ray, is confined to the plane defined by $m(\sigma_0)$ and ∇v . The ray is a circle in the plane defined by the ray tangent and the velocity gradient (see Fig. 2). The ray normal is given by

$$n(\sigma) = \cotg\theta m(\sigma) - \frac{1}{\|\nabla v\| \sin\theta} \nabla v \quad (19)$$

where θ is the angle between the ray tangent and the velocity gradient.

It can easily be shown that a point on the ray has coordinates

$$x(\sigma) = x(\sigma_0) + \rho \left[\sin \frac{\sigma - \sigma_0}{\rho} m(\sigma_0) + (1 - \cos \frac{\sigma - \sigma_0}{\rho}) n(\sigma_0) \right] \quad (20)$$

and the ray tangent is

$$m(\sigma) = \cos \frac{\sigma - \sigma_0}{\rho} m(\sigma_0) + \sin \frac{\sigma - \sigma_0}{\rho} n(\sigma_0) \quad (21)$$

Here

$$\rho = \frac{v(\sigma)}{\|\nabla v\| \sin\theta(\sigma)} \quad (22)$$

is the constant radius of ray curvature.

By using the relation $d\sigma = \rho d\theta$ and equation (22) the travel time, given in equation (3), becomes

$$t(\sigma) = t(\sigma_0) + \int_{\theta(\sigma_0)}^{\theta(\sigma)} \frac{d\theta}{\|\nabla v\| \sin\theta} = t(\sigma_0) + \frac{1}{\|\nabla v\|} \ln \frac{\tg \frac{1}{2}\theta(\sigma)}{\tg \frac{1}{2}\theta(\sigma_0)} \quad (23)$$

Since $\nabla v = \text{constant}$ equation (7) gives $C = 0$, so that equation (8) becomes

$$\frac{dG}{d\sigma} - vI = 0 \quad (24)$$

which has the solution

$$G(\sigma) = G(\sigma_0) + \int_{\sigma_0}^{\sigma} v(\xi) d\xi \cdot I \quad (25)$$

(This is equation (41) in Hubral (1980).) An explicit solution of equation (25) can be found by noting that $d\sigma = \rho d\theta$ and using equation (22) for $v(\sigma)$. This gives

$$\int_{\sigma_0}^{\sigma} v(\xi) d\xi = \rho^2 \|\nabla v\| \int_{\theta(\sigma_0)}^{\theta(\sigma)} \sin\theta d\theta \quad (26)$$

so that equation (25) becomes

$$G(\sigma) = G(\sigma_0) + \rho^2 \|\nabla v\| [\cos\theta(\sigma_0) - \cos\theta(\sigma)] \cdot I \quad (27)$$

The equations for the transformation of the wavefront curvature matrix at an interface between two media with constant velocity gradients cannot be much simplified from the general case of inhomogeneous media. The only simplification is that the velocity gradients are constant and need not be evaluated at each point of the interface.

In the derivation above we have assumed that $\sin\theta \neq 0$. In the case that $\sin\theta = 0$, the ray is a straight line parallel to the velocity gradient and we can write the velocity function as

$$v(\sigma) = v(\sigma_0) + \nabla v^T_m (\sigma - \sigma_0) \quad (28)$$

We have

$$\frac{dv}{d\sigma} = \nabla v^T_m \quad (29)$$

so that the travel time given in equation (3) becomes

$$t(\sigma) = t(\sigma_0) + \int_{v(\sigma_0)}^{v(\sigma)} \frac{dv}{v \nabla v^T \mathbf{T}_m} = t(\sigma_0) + \frac{1}{\nabla v^T \mathbf{T}_m} \ln \frac{v(\sigma)}{v(\sigma_0)} \quad (30)$$

In this case equation (25) can be integrated directly when equation (28) is used. We obtain

$$G(\sigma) = G(\sigma_0) + [v(\sigma_0)(\sigma - \sigma_0) + \frac{1}{2} \nabla v^T \mathbf{T}_m (\sigma - \sigma_0)^2] \mathbf{I} \quad (31)$$

General inhomogeneous medium

For a general inhomogeneous medium we must solve equations (1a), (1b) and (8) numerically. We have considered both the Runge-Kutta method and the Adams method. The first-mentioned is the simplest and in some respects the best understood, but it is the least efficient. We have chosen to use a modified divided difference form of the Adams PECE (Predict-Evaluate-Correct-Evaluate) formulas and local extrapolation. To describe the algorithm briefly, we introduce the initial-value problem

$$\begin{aligned} y'(x) &= f(x, y(x)) \\ y(a) &= A \\ x &\in [a, b] \end{aligned} \quad (32)$$

where y , A and f in general may be vectors.

We want to approximate the solution on a mesh, generally separated by unequal step sizes h_1, h_2, h_3, \dots so that

$$\begin{aligned} x_0 &= a \\ x_n &= x_{n-1} + h_n \quad n = 1, 2, \dots \end{aligned} \quad (33)$$

Let y_n be an approximation to the solution $y(x)$ of equation (32) at the mesh point x_n :

$$y_n \approx y(x_n) \quad (34)$$

Because $y(x)$ satisfies (32), an approximation of $y(x_n)$ leads to an approximation of $y'(x_n)$, namely:

$$f_n = f(x_n, y_n) \approx y'(x_n) = f(x_n, y(x_n)) \quad (35)$$

The basic computational task is to advance the numerical solution to x_{n+1} after having computed y_0, y_1, \dots, y_n . Any solution of equations (32) can be written as

$$y(x_{n+1}) = y(x_n) + \int_{x_n}^{x_{n+1}} y'(t) dt = y(x_n) + \int_{x_n}^{x_{n+1}} f(t, y(t)) dt \quad (36)$$

The Adams method approximates this solution by replacing $f(t, y(t))$ with an interpolating polynomial, computed from derivative values, f_j , and then integrating the polynomial.

The Adams-Bashforth formula of order k at x_n uses a polynomial $P_{k,n}(x)$ interpolating the computed derivatives at the k preceding points,

$$P_{k,n}(x_{n+1-j}) = f_{n+1-j}, \quad j = 1, 2, \dots, k \quad (37)$$

These derivatives and y_n must be stored from the preceding step. An approximation to the solution at x_{n+1} is obtained from

$$y_{n+1} = y_n + \int_{x_n}^{x_{n+1}} P_{k,n}(t) dt \quad (38)$$

The algorithms used are based on the divided difference form of the interpolating polynomial.

We now regard the Adams-Bashforth value y_{n+1} of equation (38) as a tentative, 'predicted' value and incorporate it into an interpolating polynomial. We rename the predicted value of equation (38) to p_{n+1} in order to avoid confusion. Using a new polynomial, $P_{k,n}^*(x)$, that also interpolates to k derivative values,

$$\begin{aligned} P_{k,n}^*(x_{n+1-j}) &= f_{n+1-j}, & j &= 1, \dots, k-1 \\ P_{k,n}^*(x_{n+1}) &= f(x_{n+1}, p_{n+1}) \end{aligned} \tag{39}$$

gives us the Adams-Moulton formula.

The approximate solution, y_{n+1} , is given by

$$y_{n+1} = y_n + \int_{x_n}^{x_{n+1}} P_{k,n}^*(t) dt \tag{40}$$

The algorithm we have used adjusts the order and step size to control the error per unit step in a generalized sense. The predictor-corrector approach is more accurate than most other known methods and therefore much better with respect to the propagation of error.

The reliability of the error estimates leads again to a more effective selection of the step size. A more detailed description of theory and algorithms can be found in Shampine and Allen (1973) and Shampine and Gordon (1975).

The numerical algorithms described above will also be used in integrating the direction of vectors e_1 and e_2 (see Červený and Hron, 1980).

The integration of the wavefront curvatures must be performed together with the integration of the ray-tracing system and the vectors e_1 and e_2 . This is due to the fact that we need to calculate the second derivatives of the velocity with respect to q_1 and q_2 (see for instance equation (7)) at points along the ray. Both e_1 , e_2 and the position of the ray must be known in order to evaluate these derivatives. Thus, to perform the dynamic ray-tracing in a general model, we need to integrate simultaneously 10 equations. The functions y and f and the initial condition A in equation (32) are thus vectors with dimension 10.

3-D MODEL REPRESENTATION

Representing the Interfaces

We shall now treat the problem of how to represent a 3-D model. Before turning to the detailed procedure, we shall state the following requirements:

- i) The model representation should be general enough to include models of relatively high complexity (faults, discontinuities, continuously varying velocity gradients, smooth surfaces of any curvatures, etc.).
- ii) Enough information should be specified to assure that a ray starting from an arbitrary point in the model can be effectively traced through the model, being reflected/refracted at the proper interfaces.
- iii) The manual effort in specifying the model parameters should be kept within reasonable limits.

We define the space of definition of the model as

$$S_d = \{(x_1, x_2, x_3) | (x_1, x_2) \in [a, b] \times [c, d]\} \quad (41)$$

where (x_1, x_2) are the horizontal coordinates and x_3 is the depth coordinate. We call the rectangle $[a, b] \times [c, d]$ the rectangle of definition or just R_d .

All points (x_1, x_2, x_3) with horizontal coordinates not inside the rectangle of definition are defined to be outside the model. The depth boundaries are defined by the interfaces.

To perform the dynamic ray-tracing we must claim that the interfaces are continuous and have continuous 1st and 2nd derivatives almost everywhere on R_d . Generally this condition is satisfied if we represent the interfaces by spline functions (Ahlberg et al, 1967; Gjøystdal, 1979; Gjøystdal and Ursin, 1981).

In the description of the spline functions we will for convenience use coordinates (x,y,z) instead of (x_1,x_2,x_3) . The general bicubic spline surface is specified by the z -values on a uniform rectangular grid in the xy -plane (see Fig. 3).

$$z = z(x,y) , \quad (x,y) \in [a,b] \times [c,d]$$

Sample points (x_i, y_j, z_{ij}) are given as follows:

$$x_i = x_1 + (i-1) \Delta x \quad i = 1, n \quad (42)$$

$$y_j = y_1 + (j-1) \Delta y \quad j = 1, m$$

z_{ij} - depth value in grid point (x_i, y_j) .

A bicubic spline surface is fitted through the data points, and 16 coefficients are determined on each of the $(n-1) \cdot (m-1)$ rectangles:

For a point (x,y) located within the ij -th rectangle, that is, $x_i < x < x_{i+1}$ and $y_j < y < y_{j+1}$, we have

$$z(x,y) = \sum_{k=1}^4 \sum_{\ell=1}^4 c_{ijk\ell} (x-x_i)^{k-1} (y-y_j)^{\ell-1} \quad (43)$$

Note that c_{ij11} is the depth value in (x_i, y_j) , that is, $c_{ij11} = z_{ij}$.

To summarize, each interface may be described by a sequence of $16(n-1)(m-1)+6$ parameters:

$$c_1, \Delta x, n, y_1, \Delta y, m, (c_{ijk\ell}, k=1,4, \ell=1,4, i=1,n-1, j=1,m-1) \quad (44)$$

Note that the rectangle of definition of the interface function, $[a,b] \times [c,d]$, need not be equal to the rectangle $[x_1, x_n] \times [y_1, y_m]$. The latter rectangle may be contained within the former, or the opposite may be true. This means that one has the possibility of sampling the function outside the area of definition, and that one also may extrapolate the functional values outside the given grid. In the latter case the coefficients of the closest rectangle are used in the computation of the functional value.

The bicubic spline surfaces constitute basic elements in the complete build-up of the model. In order to obtain an unambiguous description of how interfaces are located relative to each other, how they intersect, and what part of the mathematical interfaces should be considered as real, physical interfaces, we have developed a special kind of 'logic system' that is very well suited for computer representation. For details we refer to GjØystdal (1979).

Representing the velocities

In performing the dynamic ray tracing in the general case we need to calculate the values of the following functions along the ray:

$$v, \quad \nabla v, \quad \frac{\partial v}{\partial u_i}, \quad \frac{\partial^2 v}{\partial u_i \partial u_j}, \quad i, j = 1, 2 \quad (45)$$

It can be shown (Červený et al, 1977) that the ray method is very sensitive to the representation of the velocity function. Especially piece-wise linear interpolation of velocity between mesh points will have unwanted effects. This causes enormous (and unrealistic) fluctuations in amplitude coefficients over an array, even though the obtained travel times seem correct. These fluctuations are due to the fact that linear interpolation causes false interfaces of the second order to appear which have great effect on the amplitude.

We therefore require that the velocity function is continuous with continuous first and second derivatives. In addition we claim that the representation of the velocity is such that the values in (45) can be estimated at any point of any ray in the model.

We propose two ways of representing the velocity. The first representation is a very simple polynomial in x, y , and z . In the case of constant velocity gradient we have

$$v(x,y,z) = a_0 + a_1x + a_2y + a_3z \quad (46)$$

and up to the second order, we get

$$v(x,y,z) = a_0 + a_1x + a_2y + a_3z + b_{11}x^2 + b_{12}xy + b_{13}xz + b_{22}y^2 + b_{23}yz + b_{33}z^2 \quad (47)$$

The case of constant velocity gradient is particularly important since we in this case have found analytical solutions of the differential equations.

The second approach is more satisfactory from a practical point of view, and includes the use of splines (Ahlberg et al, 1967). Let us assume that we know the velocity at both sides of two interfaces. The problem is how to model the velocity in the medium separated by these interfaces. Let interface 1 be described by a bicubic spline function $z_1(x,y)$ and let $v_1(x,y)$ be a bicubic spline function representing the velocity at the side of interface 1 directed towards interface 2. Further on, let $z_2(x,y)$ be a spline describing interface 2 and $v_2(x,y)$ be a spline representing the velocity at the side of interface 2 directed towards interface 1. We may then describe the velocity in the medium by

$$v(x,y,z) = v_1(x,y) + \frac{v_2(x,y) - v_1(x,y)}{z_2(x,y) - z_1(x,y)} (z - z_1(x,y)) \quad (48)$$

This is a continuous function having continuous first and second derivatives in any direction provided that the splines z_1 and z_2 do not intersect. The function has a kind of 'preferred' direction along the z -axis since the velocity variation along this direction is linear.

If we have even more knowledge of the velocity variation in the medium, the procedure can be further generalized. Assume that n interfaces are given, $z_i(x,y), i = 1, n$, with corresponding velocities $v_i(x,y)$. For given horizontal coordinates (x,y) we may now fit a cubic spline function $u_{xy}(z)$ to velocity values at various depths such that

$$u_{xy}(z_i(x,y)) = v_i(x,y), \quad i = 1, n \quad (49)$$

The velocity is then given by

$$v(x,y,z) = u_{xy}(z) \quad (50)$$

Intersection between ray and interface

In this section we shall shortly describe a special algorithm developed to find the point of intersection between the ray and the interface. In the case of a straight or circular ray and a plane interface this point may be found analytically. But, generally we need a search process to find the intersection point. We shall use a Newton algorithm, slightly modified from the one described in Gjøystdal (1979).

Let x be the coordinate of the ray and m the tangent vector at a certain time, obtained by repeatedly stepping along the ray with a pre-specified step length. The procedure can be described as follows:

- i) If the vertical distance from x to the interface is less than a given limit, δ , initiate the Newton process.
- ii) Find the point of the interface vertically below (or above) x , here denoted x_I , and compute a plane tangential to the interface at x_I .
- iii) Compute the intersection point between the tangent plane and a straight ray from x along m and store the distance, s , from x to the intersection point.
- iv) Trace the ray from x , a distance s to a new point x' with a new tangent vector m' .

- v) If the vertical distance from x' to the interface is less than a given limit, ϵ , we say that the intersection point is found.
If the vertical distance is greater than δ , stop the process.
Otherwise, define x as x' , m as m' and go to ii).

If more than one intersection point has been found, choose the one, x_F , corresponding to minimum tracing distance from the start point.

As soon as the intersection point is found, the process goes back to the original ray point x (the one immediately before entering the Newton process) and continue going stepwise along the ray, each time checking if any interface is passed by the ray which has not been taken into account earlier. The ray-tracing is stopped as soon as the last accepted intersection point x_F is passed by the ray point x .

The reason for going back to the ray point and continuing the stepwise procedure is that the geometry of the interfaces may in certain cases be such that we miss the proper interface the first time the Newton process is initiated. This may especially happen when the ray departs considerably from the vertical direction, so that the point x_I vertically below (above) the ray point x may be located relatively far from the proper intersection point. In such cases the interfaces may be so far from the ray point x that it is not included in the Newton algorithm the first time it is entered (see Fig. 4).

We have thus seen that the general problem of finding the intersection point between the ray and an interface may be solved by a numerical procedure, and that the solution generally will be accurate within certain predefined limits (dependent on the chosen value of ϵ).

Search procedure for computation of ray paths between specified source and receiver

We have developed a special search procedure in order to find ray paths connecting a given source- and receiver-position in a 3-D model. It is based on the 'shooting method', that is, we are starting in the shot point with a certain initial direction of the ray, and the ray is traced through the model until a specified 'receiver interface' has been reached. The initial ray direction is then updated and a second ray is traced through the model. The procedure is then repeated until the ray arrives sufficiently close to the specified receiver point. The procedure is described in detail in Gjøystdal (1978A,B); here we shall restrict ourselves to stating some basic properties of the method. The procedure takes advantage of a 'receiver line' running through the receiver point. The search constitutes a 'curve crawling process' along this line, using gradient calculations for updating the ray direction at each iteration step. The procedure is especially efficient when a number of receivers are distributed along a line (or continuous curve), as is usually the case in geophysical exploration. In addition, the procedure is designed to pick up the various branches of the travel time function if such branches exist, thus being able to determine all ray paths connecting source and receiver in a complex 3-D model.

It should also be mentioned that during this search procedure, no dynamic parameters (i.e., wavefront curvature, amplitude, etc.) are calculated. Such calculations are carried out only for the resulting ray paths. These rays are traced through the medium once more, and the necessary integrations are performed in order to determine the parameters wanted.

TRAVEL TIME APPROXIMATIONS

Source-receiver coordinates

The source and receiver geometry are outlined in Fig. 5. We want to compute a travel time approximation from a source at $s = (s_1, s_2, s_3)^T$ near $s_0 = (s_{01}, s_{02}, s_{03})^T$ where the local velocity is $v(s_0)$ to a receiver at $r = (r_1, r_2, r_3)^T$ near $r_0 = (r_{01}, r_{02}, r_{03})^T$ where the local velocity is $v(r_0)$. We let the local coordinates be denoted by

$$\Delta r = r - r_0 \tag{51}$$

and

$$\Delta s = s - s_0 \tag{52}$$

A quadratic approximation of the travel time from r to s is obtained by expanding the square of the travel time in a Taylor series and taking the square root of the result. This gives the approximation (Ursin, 1981C)

$$t_1(r, s) = \left\{ \left[t(r_0, s_0) + \frac{\partial t}{\partial r^T} \Delta r + \frac{\partial t}{\partial s^T} \Delta s \right]^2 + \Delta r^T A_r \Delta r + 2 \Delta r^T A_{rs} \Delta s + \Delta s^T A_s \Delta s \right\}^{\frac{1}{2}} \tag{53}$$

where the gradient vectors are

$$\frac{\partial t}{\partial r^T} = \left(\frac{\partial t}{\partial r_1}, \frac{\partial t}{\partial r_2}, \frac{\partial t}{\partial r_3} \right) \tag{54}$$

$$\frac{\partial t}{\partial s^T} = \left(\frac{\partial t}{\partial s_1}, \frac{\partial t}{\partial s_2}, \frac{\partial t}{\partial s_3} \right)$$

The second derivative matrices have elements

$$\{A_R\}_{1j} = t(r_0, s_0) \frac{\partial^2 t}{\partial r_i \partial r_j}$$

$$\{A_S\}_{1j} = t(r_0, s_0) \frac{\partial^2 t}{\partial s_i \partial s_j} \quad (55)$$

$$\{A_{RS}\}_{1j} = t(r_0, s_0) \frac{\partial^2 t}{\partial r_i \partial s_j}$$

In equation (54) and (55) and in the following, all partial derivatives are evaluated at (r_0, s_0) . A_R and A_S are 3x3 symmetric matrices, while A_{RS} is generally a 3x3 non-symmetric matrix. All travel time parameters defining the approximation $t_1(r, s)$ in equation (53), except the cross-term matrix A_{RS} , can be defined from the ray and wavefront curvature parameters (Ursin, 1981C).

A second travel time approximation may be derived by expanding the travel time in a Taylor series (Červený and Hron, 1980; equation (50) and (51)). This gives the approximation

$$t_2(r, s) = t(r_0, s_0) + \frac{\partial t}{\partial r^T} \Delta r + \frac{\partial t}{\partial s^T} \Delta s + \frac{1}{2t(r_0, s_0)} [\Delta s^T A_S \Delta s + 2\Delta r^T A_{RS} \Delta s + \Delta r^T A_R \Delta r] \quad (56)$$

Note that $t_1(r, s)$ may be obtained from $t_2(r, s)$ by taking the square root of $t_2^2(r, s)$ with higher than second-order terms in Δr and Δs neglected.

We have chosen to use the first travel time approximation because it is exact for a spherical wavefront. Numerical simulations in a two-dimensional medium with plane dipping layers (Gangi and Yang, 1976), analytic considerations for a horizontally layered medium (Ursin, 1977), and numerical calculations for a horizontally layered medium (Ursin, 1981C) indicate that this

approximation should be used. Numerical comparisons (to be given later) also indicate that this approximation should be used for inhomogeneous layered media with curved interfaces.

Midpoint - half-offset coordinates

Instead of expressing the travel time for a specific reflection as a function of source and receiver coordinates, it can be expressed as a function of the midpoint coordinates

$$x = \frac{1}{2}(r + s) \tag{57}$$

and half the difference between the source and receiver coordinates or the half-offset coordinates

$$y = \frac{1}{2}(s - r) \tag{58}$$

From equations (57) and (58) we obtain

$$\begin{aligned} r &= x - y \\ s &= x + y \end{aligned} \tag{59}$$

We let x_0 and y_0 be defined in terms of r_0 and s_0 by equation (7) and (8). The local coordinates in the new coordinate system are

$$\begin{aligned} \Delta x &= x - x_0 \\ \Delta y &= y - y_0 \end{aligned} \tag{60}$$

The first travel time approximation can now be expressed by

$$\begin{aligned} t_1(x,y) &= \left\{ \left[t(x_0, y_0) + \frac{\partial t}{\partial x^T} \Delta x + \frac{\partial t}{\partial y^T} \Delta y \right]^2 + \Delta x^T B_x \Delta x \right. \\ &\quad \left. + 2\Delta x^T B_{xy} \Delta y + \Delta y^T B_y \Delta y \right\}^{\frac{1}{2}} \end{aligned} \tag{61}$$

where the gradient vectors are

$$\frac{\partial t}{\partial x} = \frac{\partial t}{\partial r} + \frac{\partial t}{\partial s} \quad (62)$$

$$\frac{\partial t}{\partial y} = \frac{\partial t}{\partial s} - \frac{\partial t}{\partial r}$$

and the second-derivative matrices B_x , B_{xy} and B_y have elements

$$\{B_x\}_{ij} = t(x_0, y_0) \frac{\partial^2 t}{\partial x_i \partial x_j}$$

$$\{B_{xy}\}_{ij} = t(x_0, y_0) \frac{\partial^2 t}{\partial x_i \partial y_j} \quad (63)$$

$$\{B_y\}_{ij} = t(x_0, y_0) \frac{\partial^2 t}{\partial y_i \partial y_j}$$

respectively. We note that (Ursin, 1981C)

$$\begin{aligned} B_x &= A_r + A_s + A_{rs} + A_{rs}^T \\ B_y &= A_r + A_s - A_{rs} - A_{rs}^T \\ B_{xy} &= A_s - A_r + A_{rs} - A_{rs}^T \end{aligned} \quad (64)$$

and also that B_x and B_y are always symmetric matrices.

We see that the travel time approximation expressed in midpoint - half-offset coordinates offers no possibility for simplification in the case of a non-normal incidence ray (that is, $r_0 \neq s_0$ or $y_0 \neq 0$). On the contrary, the second-derivative matrices are now related to the wavefront curvature matrices in a more complicated way than when the source-receiver coordinates are used.

The second travel time approximation can also be expressed in midpoint - half-offset coordinates. This gives

$$t_2(x,y) = t(x_0,y_0) + \frac{\partial t}{\partial x^T} \Delta x + \frac{\partial t}{\partial y^T} \Delta y + \frac{1}{2t(x_0,y_0)} [\Delta x^T B_x \Delta x + 2\Delta x^T B_{xy} \Delta y + \Delta y^T B_y \Delta y] \quad (65)$$

Zero-offset approximations

When the reference source and receiver are located at the same point ($r_0 = s_0 = x_0$ and $y_0 = 0$), the reference ray is a normal-incidence ray. We then have

$$\frac{\partial t}{\partial r} = \frac{\partial t}{\partial s} \quad (66)$$

which gives (see equation (62))

$$\frac{\partial t}{\partial x} = 2 \frac{\partial t}{\partial r} \quad (67)$$

and

$$\frac{\partial t}{\partial y} = 0 \quad (68)$$

With

$$\frac{\partial t(x,0)}{\partial y_i} = 0$$

for all values of x , we obtain $\frac{\partial^2 t(x,0)}{\partial y_i \partial x_j} = 0$ or $B_{xy} = 0$.

This implies that $A_{rs} = A_{rs}^T$ since we have, by construction, $A_r = A_s$ for zero offset.

In source-receiver coordinates we then obtain

$$t_1(r,s) = \left\{ \left[t(r_0, r_0) + \frac{\partial t}{\partial r^T} \Delta r + \frac{\partial t}{\partial r^T} \Delta s \right]^2 + \Delta r^T A_r \Delta r + 2\Delta r^T A_{rs} \Delta s + \Delta s^T A_r \Delta s \right\}^{\frac{1}{2}} \quad (69)$$

where A_r and A_{rs} are symmetric matrices. In midpoint - half-offset coordinates we have

$$t_1(x,y) = \left\{ \left[t(x_0, 0) + \frac{\partial t}{\partial x^T} \Delta x \right]^2 + \Delta x^T B_x \Delta x + y^T B_y y \right\}^{\frac{1}{2}} \quad (70)$$

where $\frac{\partial t}{\partial x}$ is given in equation (67) and

$$\begin{aligned} B_x &= 2A_r + 2A_{rs} \\ B_y &= 2A_r - 2A_{rs} \end{aligned} \quad (71)$$

The second travel time approximation becomes, for zero-offset,

$$\begin{aligned} t_2(r,s) &= t(r_0, s_0) + \frac{\partial t}{\partial r^T} \Delta r + \frac{\partial t}{\partial r^T} \Delta s \\ &+ \frac{1}{2t(r_0, s_0)} \left[\Delta r^T A_r \Delta r + 2\Delta r^T A_{rs} \Delta s + \Delta s^T A_r \Delta s \right] \end{aligned} \quad (72)$$

In midpoint - half-offset coordinates this is

$$t_2(x,y) = t(x_0, 0) + \frac{\partial t}{\partial x^T} \Delta x + \frac{1}{2t(x_0, 0)} \left[\Delta x^T B_x \Delta x + y^T B_y y \right] \quad (73)$$

We see that in equation (70) and (73) all first-order terms of y are zero.

For a medium consisting of homogeneous layers and plane dipping interfaces we have $B_x=0$ for the zero-offset approximations (Ursin, 1981C). This gives the simplified expressions

$$t_1(x,0) = \left\{ [t(x_0,0) + \frac{\partial t}{\partial x^T} \Delta x]^2 + y^T B_y y \right\}^{\frac{1}{2}} \quad (74)$$

and

$$t_2(x,0) = t(x_0,0) + \frac{\partial t}{\partial x^T} \Delta x + \frac{1}{2t(x_0,0)} y^T B_y y \quad (75)$$

As mentioned previously, the cross-term matrix A_{rs} cannot generally be calculated from the ray and wavefront parameters of the reference ray, which means that this matrix has to be determined by numerical approximations (i.e., by tracing additional rays in the vicinity of the reference ray). From eq. (64) we may then conclude that the calculation of matrices B_x , B_y , and B_{xy} are generally subject to the same limitations. However, a very interesting feature is to be observed in the zero-offset case. It turns out that the matrix B_x (see eq. (63)) can then be calculated from parameters associated with the reference ray only. B_x can be found by tracing a number of NIP rays close to the reference NIP ray and computing the second-derivatives of the travel time function. This corresponds to starting at the foot point (reflection point) of the normal incidence ray with a wavefront matrix identical to the curvature matrix of the reflecting interface at this point. Computing this wavefront along the NIP ray up to the surface, the resulting wavefront matrix will have exactly the same relation to B_x as the wavefront matrix traced from the source has to the matrix A_r (see equations (55) and (63)). By computing the matrix A_r from the wavefront computed from source to receiver along the NIP ray and the matrix B_x by the procedure just mentioned, we are able to calculate all matrices A_r , A_{rs} , B_x , and B_y from parameters tied to the reference ray only (see equation (71)).

Having obtained the matrix B_y , it is possible to calculate 'theoretical stacking velocities' in the reference point (i.e., source/receiver point). Setting $\Delta x = 0$ in eq. (70) we have

$$t_1(y) = [t(x_0,0)^2 + y^T B_y y]^{\frac{1}{2}} \quad (76)$$

Assuming $y^T = (y_1, y_2, 0)$ (i.e., source and receiver are confined to the horizontal plane) we may write (76) as

$$t_1(y)^2 = t(x_0, 0)^2 + B_{y11}y_1^2 + 2B_{y12}y_1y_2 + B_{y22}y_2^2 \quad (77)$$

Setting

$$y_1 = \|y\| \cos\theta \quad (78)$$

$$y_2 = \|y\| \sin\theta$$

eq. (77) may be written

$$t_1(y)^2 = t(x_0, 0)^2 + \frac{(2\|y\|)^2}{v_s^2(\theta)} \quad (79)$$

$$\text{where } v_s(\theta) = \frac{1}{2}(B_{y11}\cos^2\theta + 2B_{y12}\sin\theta\cos\theta + B_{y22}\cos^2\theta)^{-\frac{1}{2}} \quad (80)$$

$v_s(\theta)$ is the stacking velocity in a direction making an angle θ with the x-axis, and $2\|y\|$ is the shot/receiver distance.

By diagonalization of the (2x2) matrix (the prime is used to separate it from the (3x3) matrix B_y)

$$B'_y = \begin{bmatrix} B_{y11} & B_{y12} \\ B_{y21} & B_{y22} \end{bmatrix} \quad (81)$$

we may thus find two principal stacking velocities v_{s1} and v_{s2} and the corresponding angles of rotation θ_1 and θ_2 .

NUMERICAL RESULTS

In this section we shall give a number of numerical results from the dynamic ray-tracing system developed, and thus investigate the accuracy and range of validity of the simplified travel time approximations for different 3-D models. We will consider the normal incidence case only, in which stacking velocities can be calculated theoretically by use of the matrix B_y .

We have investigated a number of 3-D models, comprising

- horizontal reflectors
 - plane, dipping reflectors
 - generally curved reflectors
- and various velocity functions, such as
- constant velocity
 - constant velocity gradient
 - second order polynomials in space coordinates x_1 , x_2 , and x_3 .

Zero offset case

In all examples that will be shown for the zero offset case, we start with the horizontal source/receiver configuration shown in Fig. (6). This configuration constitutes a 3-D CDP-family of rays centered about the reference point, in which source and receiver coincide. It is seen that the source/receiver points are grouped in 6 different directions, each separated by an angle of 30 degrees in the horizontal plane. This configuration will permit 6 conventional velocity analyses to be carried out in order to estimate stacking velocities for different azimuths.

For a given reflector, rays corresponding to the above source/receiver configuration are traced through the model, and the travel times are calculated.

For the central ray two different wavefront calculations are performed:

- 1) Starting in the source point with wavefront radius matrix = 0, we trace the wavefront along the normal incidence ray and thus calculate the matrix A_r at the receiver.

- 2) Starting in the NIP reflection point with wavefront curvature equal to interface curvature, we trace the wavefront up to the receiver and thus calculate the matrix B_x , and thereby the matrix B_y from eq. (71).

We now calculate the two travel time approximations t_1 and t_2 from eqs. (70) and (73). The time errors are given by

$$\Delta t_1(y_1, y_2) = t - t_1(y_1, y_2) \quad (82)$$

$$\Delta t_2(y_1, y_2) = t - t_2(y_1, y_2)$$

where t is the actual travel time found by ray-tracing between the non-zero offset points. A contour map of the time errors can now be constructed.

In each of the 6 directions defined by the source/receiver configuration, we then calculate a pair of $(t(0), v_g)$ by linear least square fit of the well-known formula

$$t(y_k)^2 \approx t(0)^2 + \frac{(2\|y_k\|)^2}{v_g^2} \quad (83)$$

where $y_k = (y_{k1}, y_{k2})^T$, and $t(y_k)$ and $2\|y_k\|$ are calculated travel time and source/receiver distance for the different source/receiver pairs within the direction considered.

From the 6 estimated pairs of $(t(0), v_g)$ (one for each direction), we may obtain estimates of the three components B_{y11} , B_{y12} , and B_{y22} of the matrix B_y . This is achieved by solving a set of 6 linear equations by a generalized least squares procedure (see f.ex. Lanczos, 1961; Golub and Reinsch, 1970). Finally, we get estimates of the principal stacking velocities v_{g1} and v_{g2} and the corresponding principal directions θ_1 and θ_2 (see eq. (81)).

In this way we obtain a 'best fit' wavefront. Using eq. (70) again with the estimated values of B_y instead of the ones calculated from the wavefront curvatures, we obtain the time error:

$$\Delta t_1'(y_1, y_2) = t - t_1'(y_1, y_2) \quad (84)$$

By assuming horizontal layers we may compute a single stacking velocity for the whole 3-D spread. It is computed by putting all the data (i.e., data from all directions) into a least squares procedure. This velocity will be denoted by \bar{v}_s in the following. We may then compute the time error associated with the 'best fit' single velocity \bar{v}_s :

$$\Delta t_1''(y_1, y_2) = t - \sqrt{t(0)^2 + \frac{(2\|y\|)^2}{\bar{v}_s^2}} \quad (85)$$

The results from these calculations are given in Figs. 7 to 14. Each figure consists of 7 displays, each being associated with a certain CDP spread in one of the models. Within each figure the displays are denoted by a letter A-G. The same letter always refers to the same type of display.

In A we display a vertical cross-section through the model in the x-direction (x and y are horizontal coordinates). Superimposed are the projection into this cross-section of the rays used for the analysis (i.e., the 3-D CDP family of rays about the reference point). We have also given the velocity functions in each layer.

In D, E, F, and G we display a map of travel time errors Δt_1 , Δt_2 , $\Delta t_1'$, $\Delta t_1''$, respectively (see eqs. (82), (84), and (85)) as a function of half-offset coordinates y_1 and y_2 .

In B we show the time errors for all data points as a function of source/receiver distance, using the estimated 'best fit' values of B_y . This display should be compared to C, in which we show time errors using the single

stacking velocity \bar{v}_s . This should demonstrate to what extent one may use different directions in the same velocity analysis, as is sometimes done in 3-D seismic processing.

For the sake of completeness we have shown all types of displays even for the very simple models, although some of these results are trivial. This is for example the case in Fig. 7, where all time errors are zero except for approximation 2, which is very bad. This simply reflects the fact that approximation 1 is exact in a homogeneous medium, whereas the Taylor expansion giving approximation 2 is not valid for small travel distances (i.e., shallow reflectors). In Figs. 7, 8 and 9 the models vary only in the vertical direction, and the results given in B and C will be equal.

This is also the case for results given in F and G. The reason for this is of course that the stacking velocity is the same in all directions, such that we have $v_{s1} = v_{s2} = \bar{v}_s$. We will first consider the approximations tied to the theoretical wavefront calculations, i.e., the ones displayed in displays D and E. In most cases it turns out that approximation 1 is superior to approximation 2. This is especially true for relatively shallow reflectors and relatively simple models. For models with more complex velocity distributions it is rather difficult to make general conclusions. For the model in Fig. 10, which has a considerable horizontal velocity variation in the 3rd layer, the two approximations are comparable in the vicinity of the reference ray, whereas the second approximation is better than the first one further away from the reference ray. Also for the model in Fig. 14, having both generally curved interfaces and complex velocity variations, the two approximations give comparable results. For this kind of complex models, however, the behavior of the error functions is very dependent on the particular model considered, and local minima may exist (more or less by chance) at certain distances from the reference ray (see, for example, Fig. 10E).

When considering the results from the 'best fit' wavefront calculations, it may be concluded that the area of small errors (e.g., errors less than 4 msec) are considerably larger than the area corresponding to the theoretical

wavefront calculations. The reason for this is of course that in the first case, the approximations have been fitted to the true travel times, whereas the theoretical wavefronts are based on computations along the reference ray only. Thus, for complex models, the derivatives at points along the reference ray have no chance to 'predict' the model behavior when the distance from this ray increases.

CONCLUSIONS

We have developed procedures to perform dynamic ray-tracing in complex 3-D models based on the ray method. The developments have been applied to test two different travel time approximations.

We have given a quadratic approximation of the squared travel time in terms of the source and receiver coordinates and in terms of the coordinates of the midpoint between the source and the receiver and half the difference between the source and receiver coordinates. The approximations are valid for any primary or multiple reflection provided that the travel time is a continuous function. Different branches of a travel time function have to be treated by separate approximations. We have considered travel time approximations from a source region to a receiver region. We have shown that the proposed travel time approximation is exact for a plane reflecting interface in a homogeneous medium, and we have presented numerical results which suggest that the proposed travel time approximation is more accurate than a travel time approximation based on second order Taylor series expansions of the travel time.

The difference between the two approximations is particularly large for shallow reflectors, for which the wavefront curvatures are large. For deeper reflectors, the results become more comparable, and for models with complex velocity variations the second approximation may happen to be slightly better than the first one.

In the processing of three-dimensional seismic data the unknown travel time parameters for each reflected wave may be estimated by using the method of least squares as in the two-dimensional case (Ursin, 1977). The amount of measurement data and the number of unknown parameters are both larger for three-dimensional seismic processing and therefore more computer resources are required. Usually the seismic traces are sorted so that the mid-point coordinates lie in a rectangle and we can use a zero-offset approximation of the travel time as shown in equation (70). The number of unknown travel time parameters can be reduced by three if we assume that the curvature of the reflecting interfaces is small so that we can assume that $B_x = 0$. For a practical algorithm for seismic travel time parameter estimation it is therefore suggested to use the approximation in equation (74). Then 6 unknown parameters must be estimated for each primary reflected wave. These are the normal-incidence travel time, $t(x_0, 0)$, two dip-components $\partial t / \partial x$, and three unknown elements of the symmetric matrix of B_y .

In this work we have given numerical results for the zero-offset case, assuming that $\Delta x = 0$, so that all mid-points of a certain CDP-family of rays coincide. In this case, we have estimated the 4 parameters $t(0)$, B_{y11} , B_{y12} , and B_{y22} . The method we have used is not strictly optimal in the least squares sense, since we have firstly performed a conventional 2-D velocity calculation in various directions, and secondly calculated the 4 parameters mentioned. The main reason for using this procedure is that it is very convenient for use in a practical situation, using real data. By performing at least 3 conventional 2-D velocity analyses (in 3 different directions) the 4 parameters $t(0)$, B_{y11} , B_{y12} , and B_{y22} can be estimated.

REFERENCES

- Ahlberg, J.H., Nilson, E.N., and Walsh, J.L., 1967, The theory of splines and their applications: New York, Academic Press
- Červený, V., I.A. Molotkov and I. Psencik, 1977, Ray Method in Seismology: Universita Karlova, Praha.
- Červený, V., and Hron, F., 1980, The ray series method and dynamic ray tracing system for three-dimensional inhomogeneous media: Bull. Seism. Soc. Am., v. 70, p. 47-77.
- Gangi, A.F., and Yang, S.J., 1976, Travel time curves for reflections in dipping layers: Geophysics, v. 41, p. 425-440.
- Gjøystdal, H., 1978A, A general computer algorithm for calculating zero-value contours of a bivariate scalar function, with special application to seismic ray-tracing in complex 3-dimensional models: Tech. Report No. 4/80, NTN/NORSAR, Kjeller.
- Gjøystdal, H., 1978B, Computation of seismic ray paths between given source and receiver line in a complex 3-D model: Tech. Report No. 3/80, NTN/NORSAR, Kjeller.
- Gjøystdal, H., 1979, Ray tracing in complex 3-D geological models: Presented at the 49th Annual International SEG Meeting, November 5, in New Orleans.
- Gjøystdal, H., and Ursin, B., 1981, Inversion of reflection times in three dimensions: Geophysics, v. 46, p. 972-983.
- Golub, G.H., and Reinsch, C., 1970, Singular value decomposition and least squares solutions: Num. Math., v. 14, p. 403-420.
- Hubral, P., 1979, A wavefront curvature approach to computing ray amplitudes in inhomogeneous media with curved interfaces: Studia geoph. et geod., v. 23, p. 131-137.
- Hubral, P., 1980, Wavefront curvatures in three-dimensional laterally inhomogeneous media with curved interfaces: Geophysics, v. 45, p. 905-913.
- Lanczos, C., 1961, Linear differential operators: New York, Van Nostrand-Reinhold.
- Lewin, L., Chang, D.C., and Kuester, E.F., 1977, Electromagnetic waves and curved structures: London, Peter Peregrinus Ltd.

- Popov, M.M., and Pšenčík, I., 1978a, Ray amplitudes in inhomogeneous media with curved interfaces: Travaux Inst. Geophys. Acad. Tcheosl. Sci., No. 454, p. 111-129, Geofysikalni sbornik, Academia, Praha.
- Popov, M.M., and Pšenčík, I., 1978b, Computation of ray amplitudes in inhomogeneous media with curved interfaces: Studia geoph. et geod., v. 22, p. 248-258.
- Reinhardsen, J.E., 1981, Dynamic ray-tracing in complex three-dimensional geological models: Tech. Report 1/81, NTN/NORSAR, Kjeller.
- Robinson, J.C., 1970, An investigation of the relative accuracy of the most common normal moveout expression in velocity analysis: Geophys. Prosp. v. 18, p. 352-363.
- Shah, P.M., 1973, Ray tracing in three dimensions: Geophysics, v. 38, p. 600-604.
- Shampine, L.F., and Allen, R.C., 1973, Numerical Computing: An Introduction: Saunders, Philadelphia.
- Shampine, L.F., and Gordon, M.K., 1975, Computer Solution of Ordinary Differential Equations: The Initial Value Problem: W.H. Freeman & Co., San Francisco.
- Taner, M.T., Cook E.E., and Neidell, N.S., 1970, Limitations of the reflection seismic method; lessons from computer simulations: Geophysics, v. 35, p. 551-573.
- Tang, C.H., 1970, An orthogonal coordinate system for curved pipes: IEEE Trans. on Microwave Theory and Techniques, v. MTT-18, p. 69.
- Ursin, B., 1977, Seismic velocity estimation: Geophys. Prospecting, v. 25, p. 658-666.
- Ursin, B., 1981A, Time-to-depth migration using wavefront curvature: Manuscript submitted for publication.
- Ursin, B., 1981B, A new derivation of the wavefront curvature transformation at an interface between two inhomogeneous media: Manuscript submitted for publication.
- Ursin, B., 1981C, Quadratic wavefront and travelttime approximations in inhomogeneous layered media with curved interfaces: Manuscript submitted for publication

FIGURE CAPTIONS

- Fig. 1 Rays at the interface between two inhomogeneous layers.
- Fig. 2 Vectors in the plane defined by the ray tangent and the velocity gradient.
- Fig. 3 Schematic representation of a bicubic spline surface, represented by a cubic function on each separate rectangle.
- Fig. 4 Illustration of the ray/interface intersection process.
- Fig. 5 Source and receiver coordinate system.
- Fig. 6 Shot/receiver configuration used in the numerical examples.
- Fig. 7-14 A Vertical cross section through the model in the horizontal x-direction. Superimposed are the projections of the rays used for the analysis.
- B Time errors for all data points as a function of source/receiver distance, using estimated 'best fit' values of B_y .
- C Time errors for all data points as a function of source/receiver distance, using the 'overall' velocity \bar{v}_g .
- D Contour map of travel time error using time approximation I and the theoretical wavefront.
- E Contour map of travel time error using time approximation II and the theoretical wavefront.
- F Contour map of travel time error using time approximation I and the 'best fit' wavefront.
- G Contour map of travel time error using time approximation I and the 'best fit' single velocity.
- In the error maps the 4 ms contours are indicated by heavy lines. In the model of Fig. 11A, the reflecting layer is dipping in the y-direction with slope = 0.1. The 3-D model of Figs. 12-14 is shown in Fig. 15.

Fig. 15 Three dimensional plot of the model used in Figs. 12-14. Vertical scale is exaggerated. Horizon extension is 10x10 km; vertical extension is 4 km.



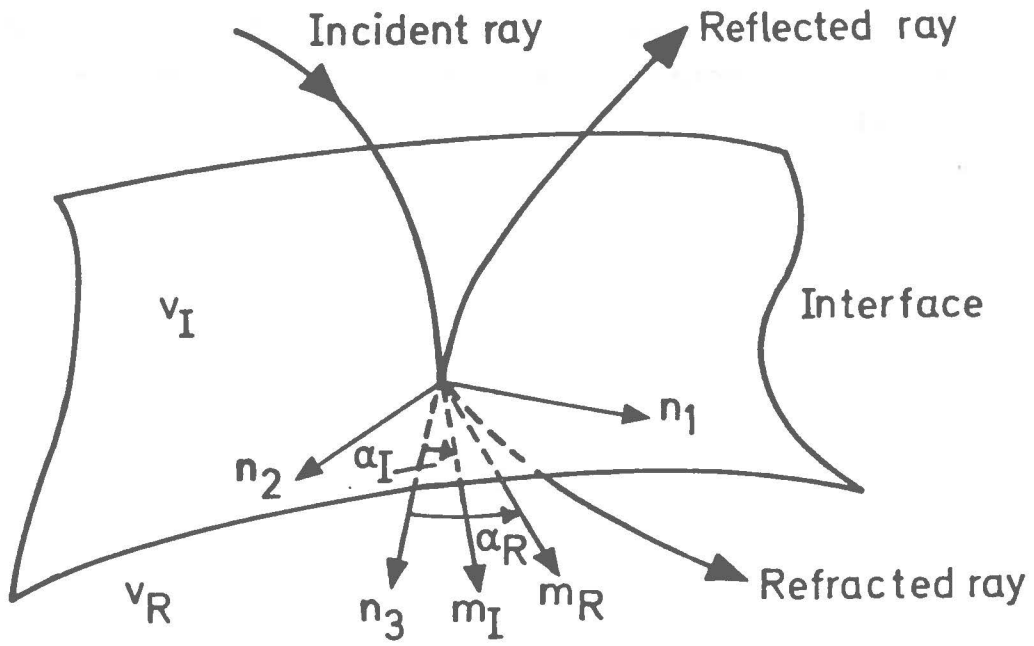


Fig.1

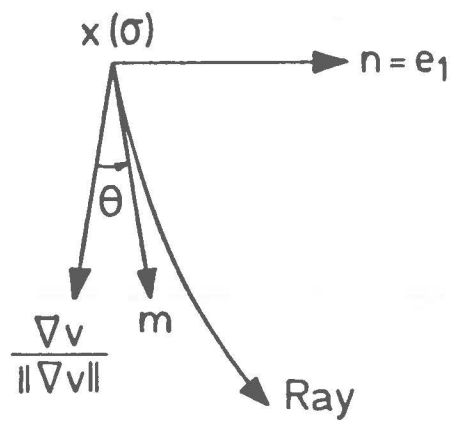


Fig.2

Fig. 4

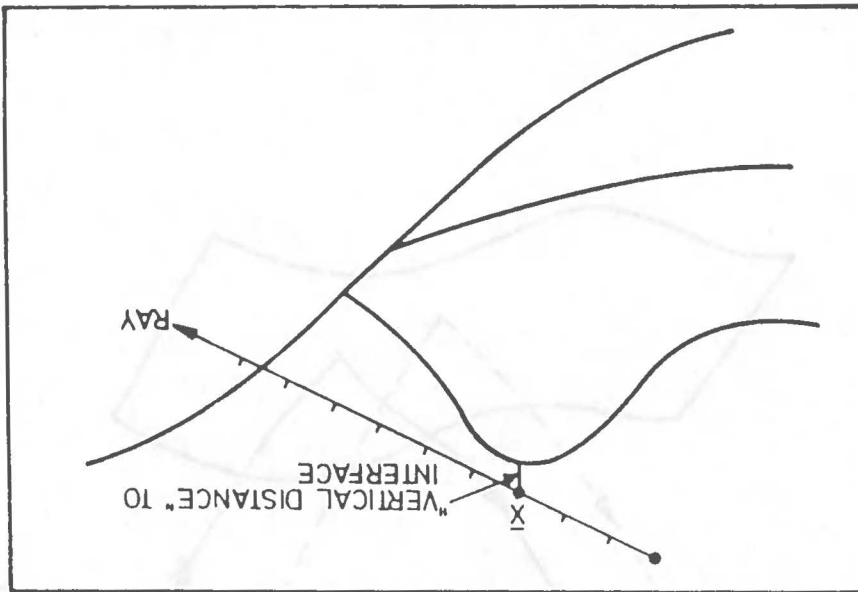
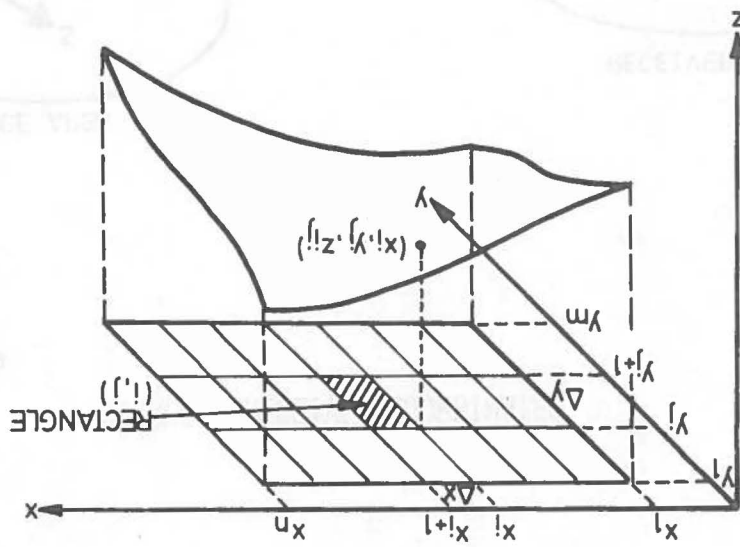


Fig. 3



SOURCE - RECEIVER COORDINATES

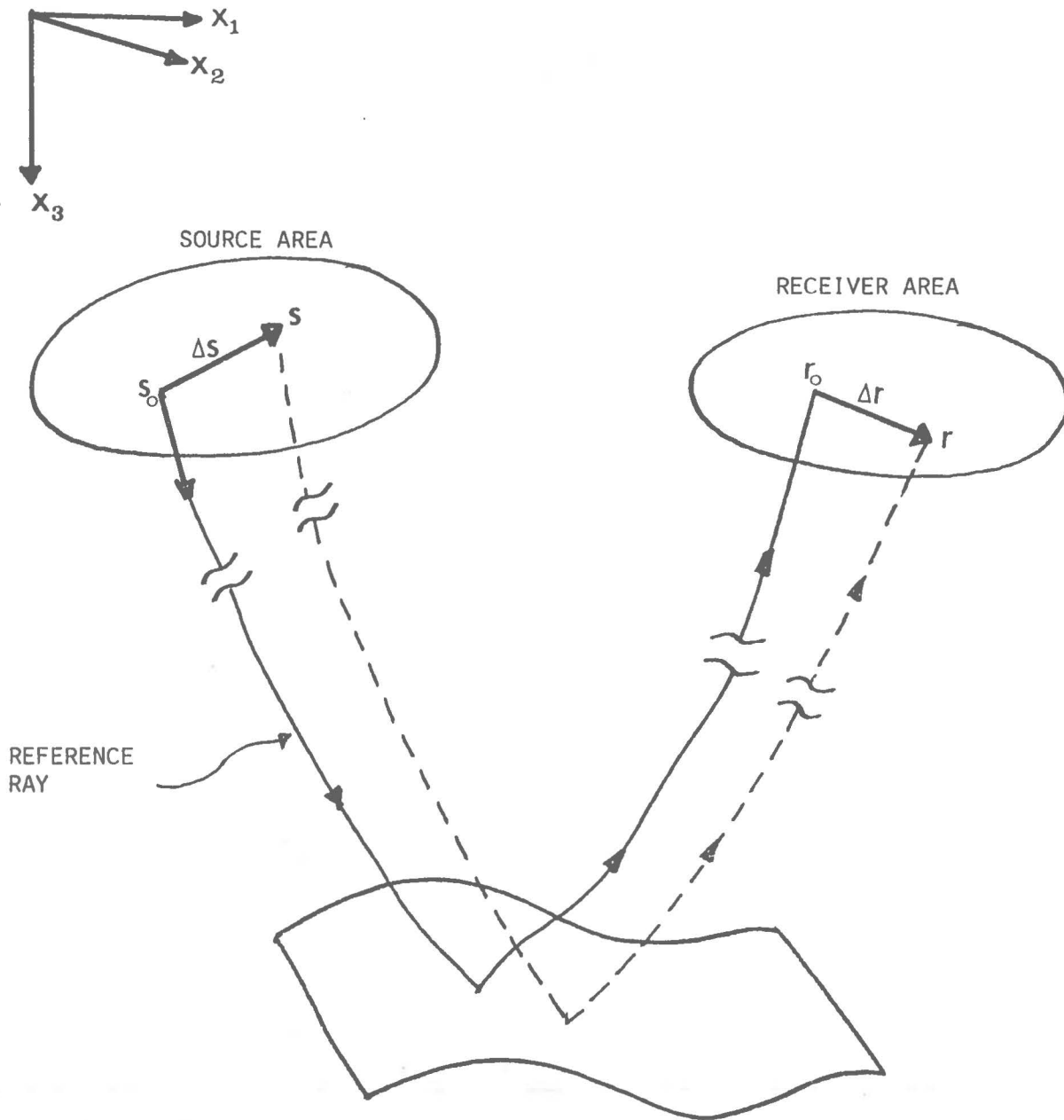


Fig.5

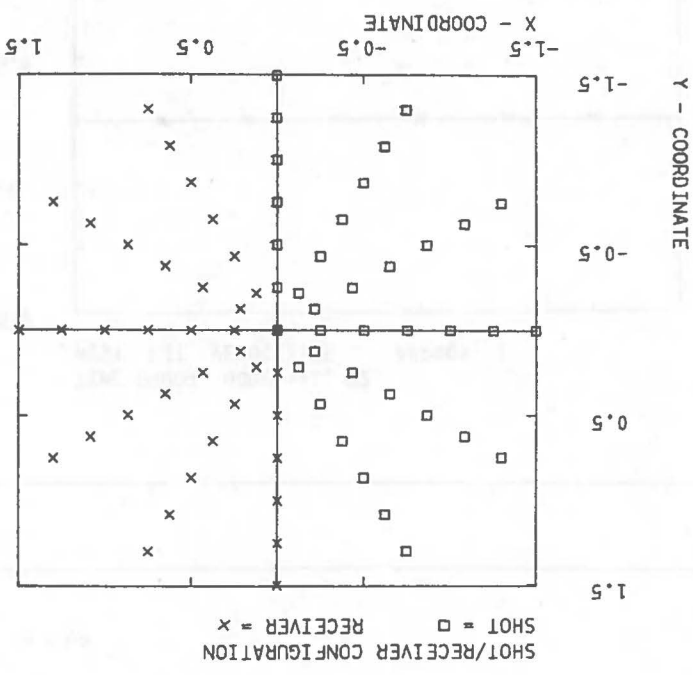


Fig. 6

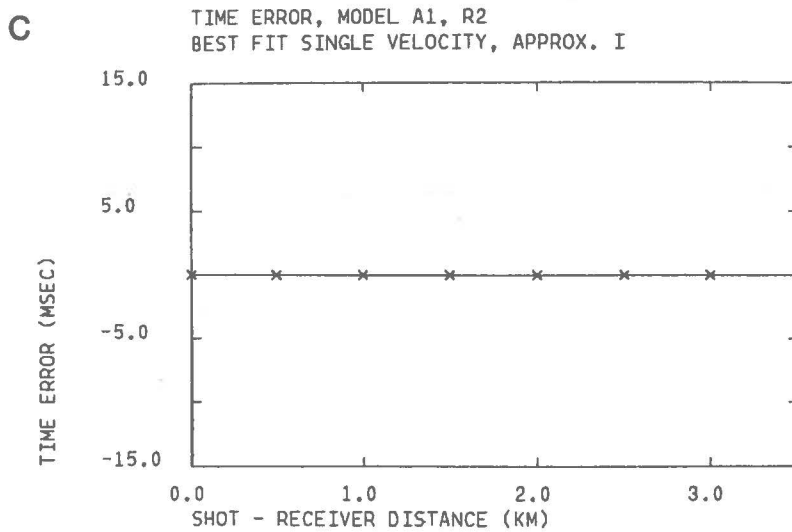
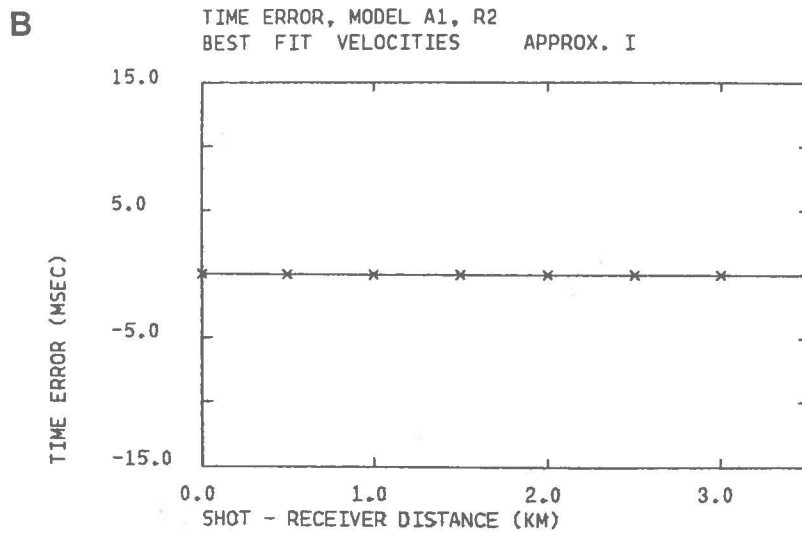
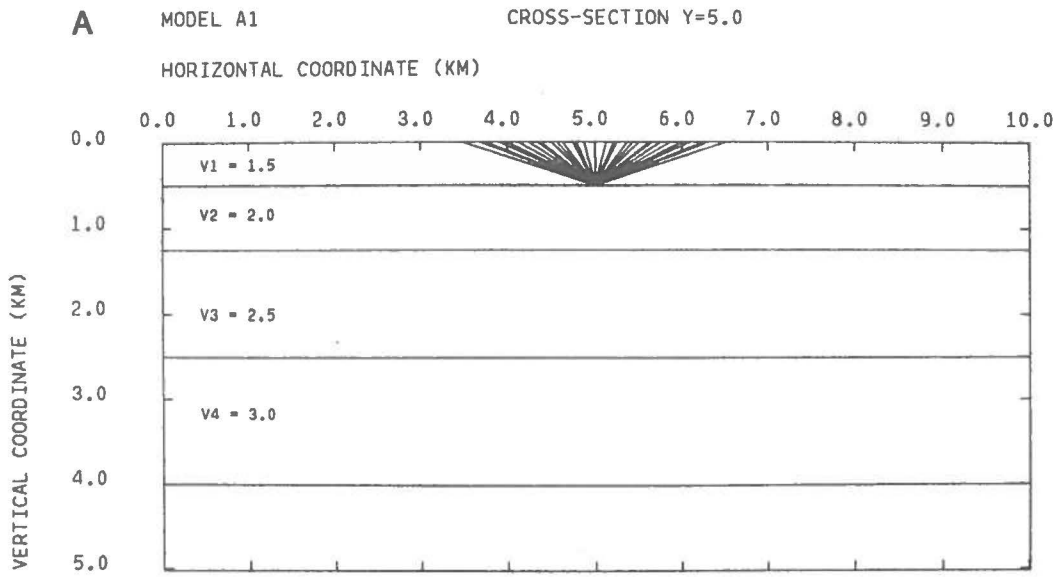


Fig.7

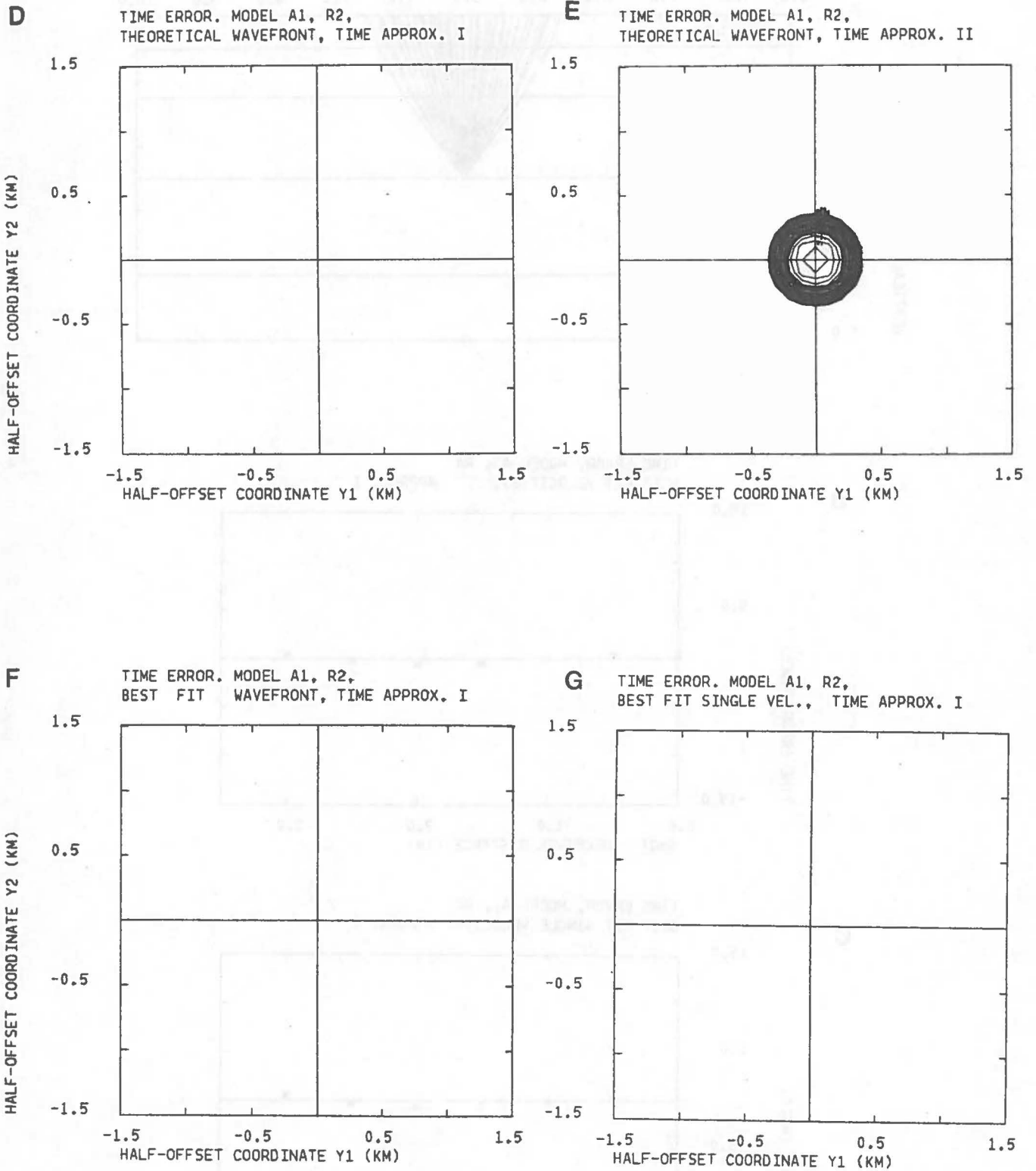


Fig.7

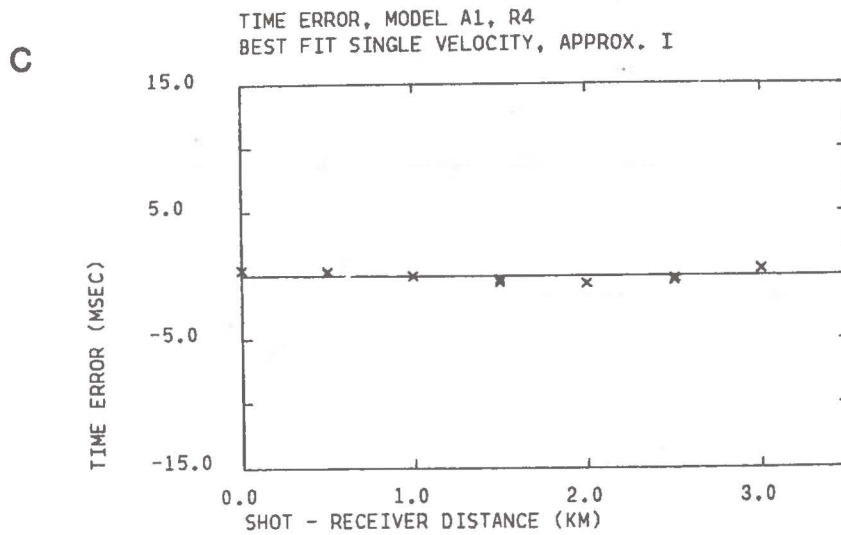
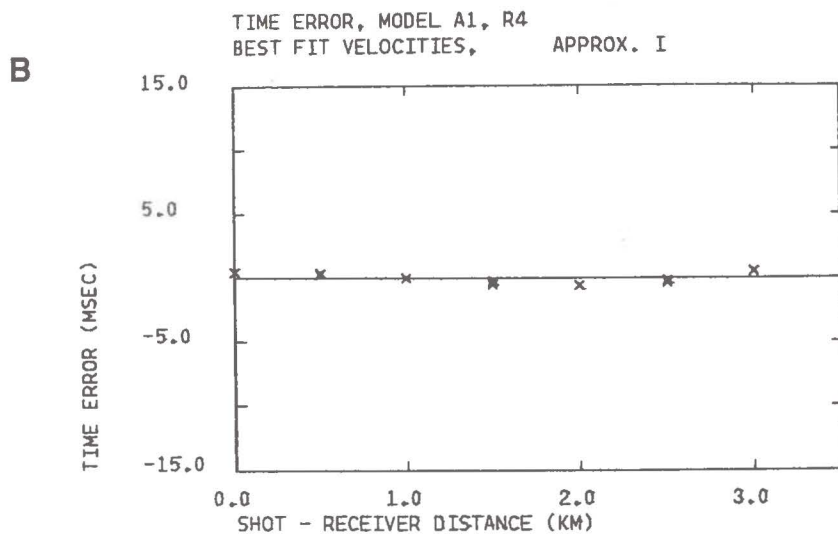
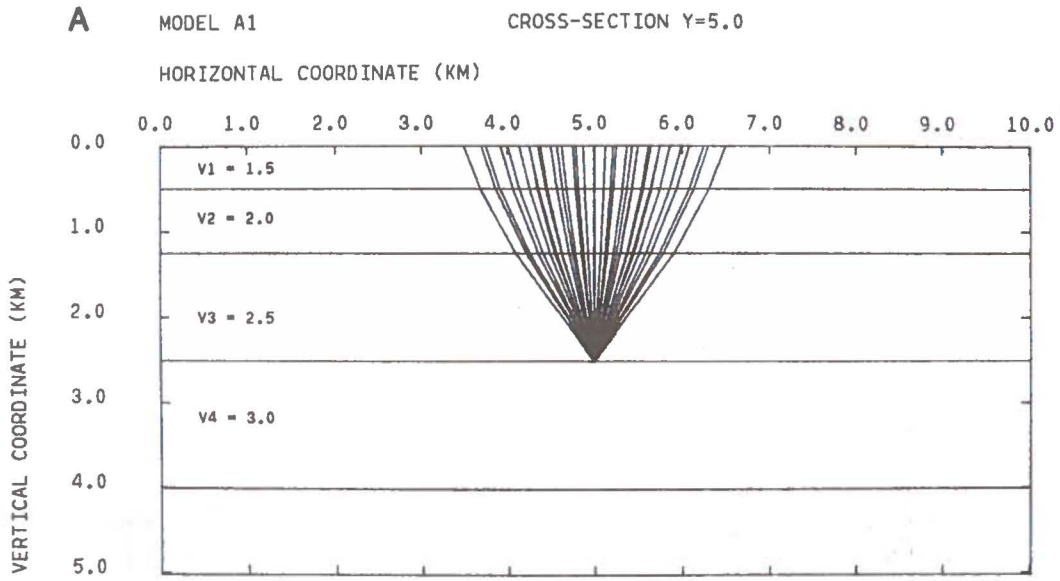


Fig.8

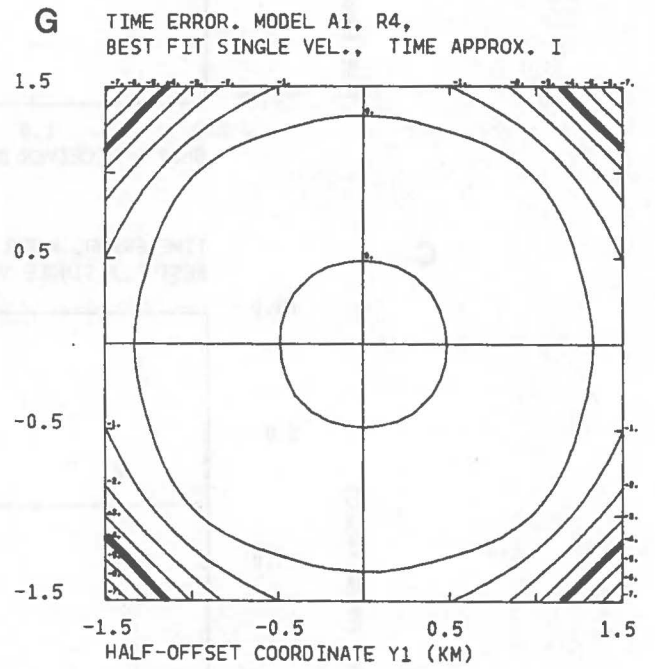
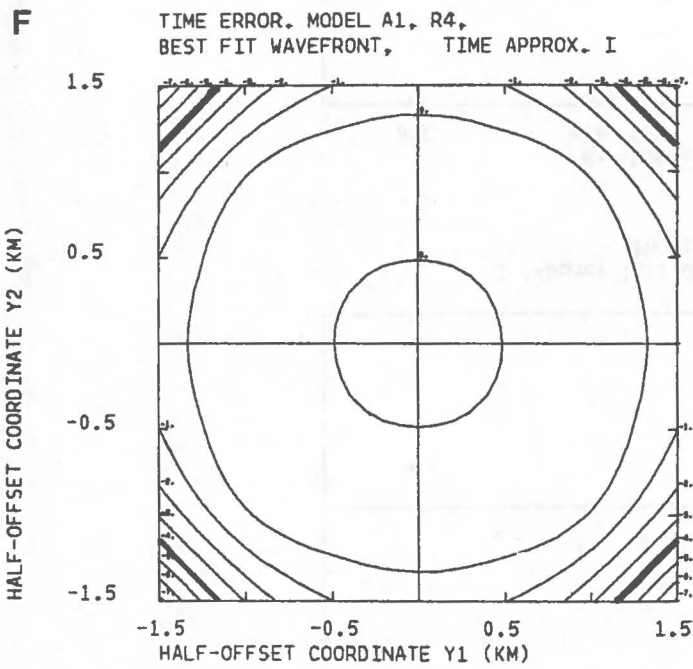
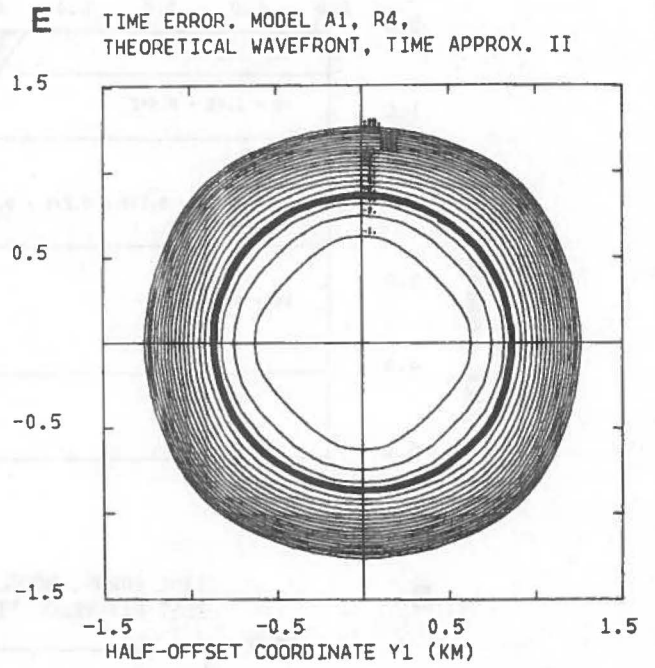
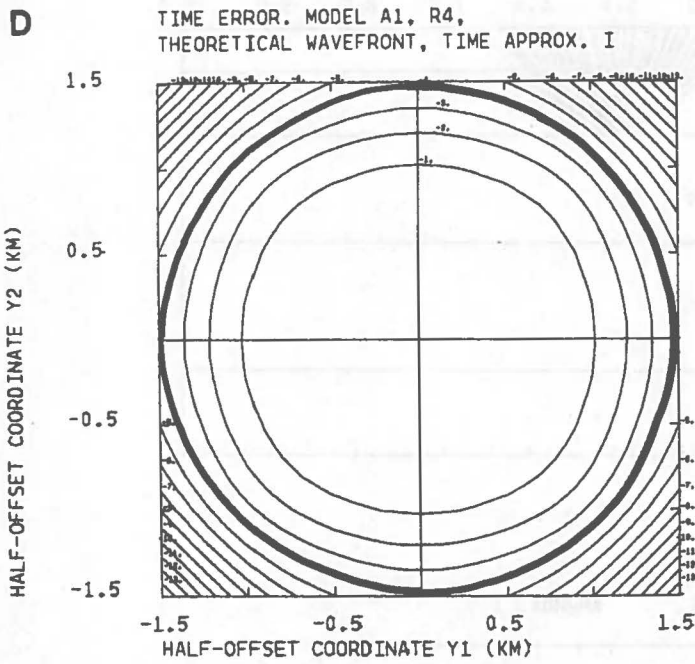


Fig.8

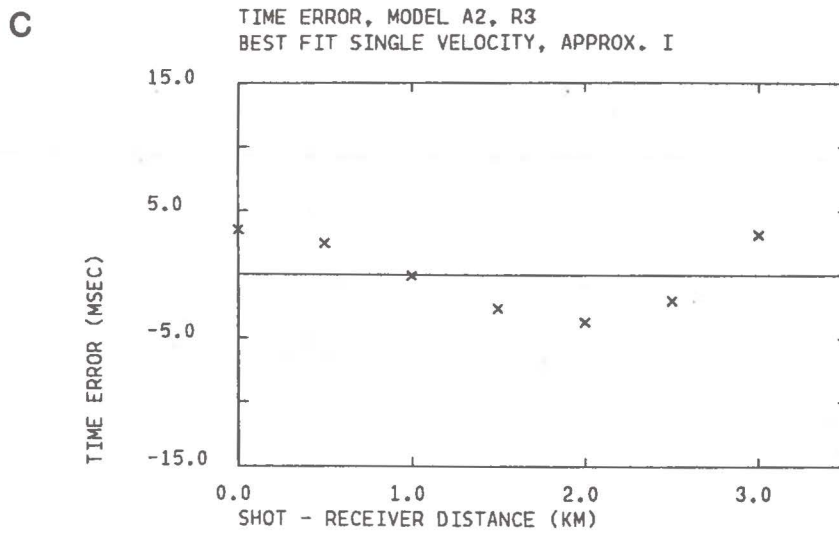
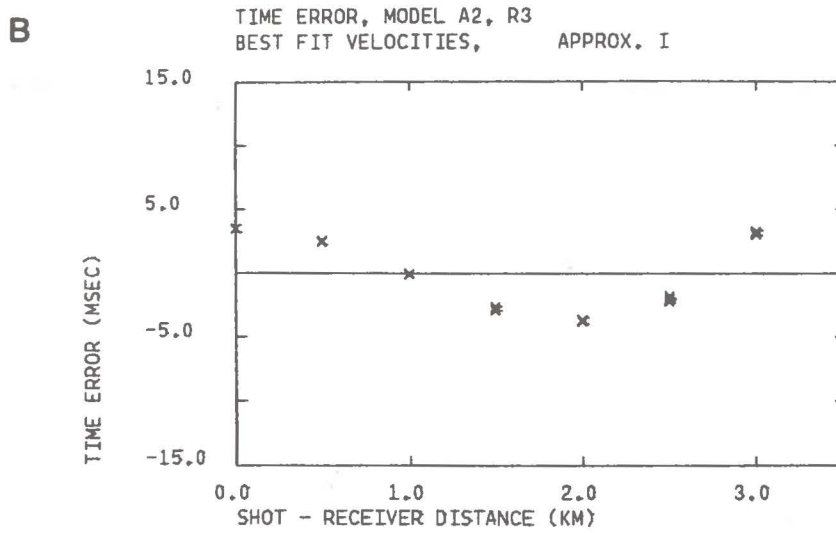
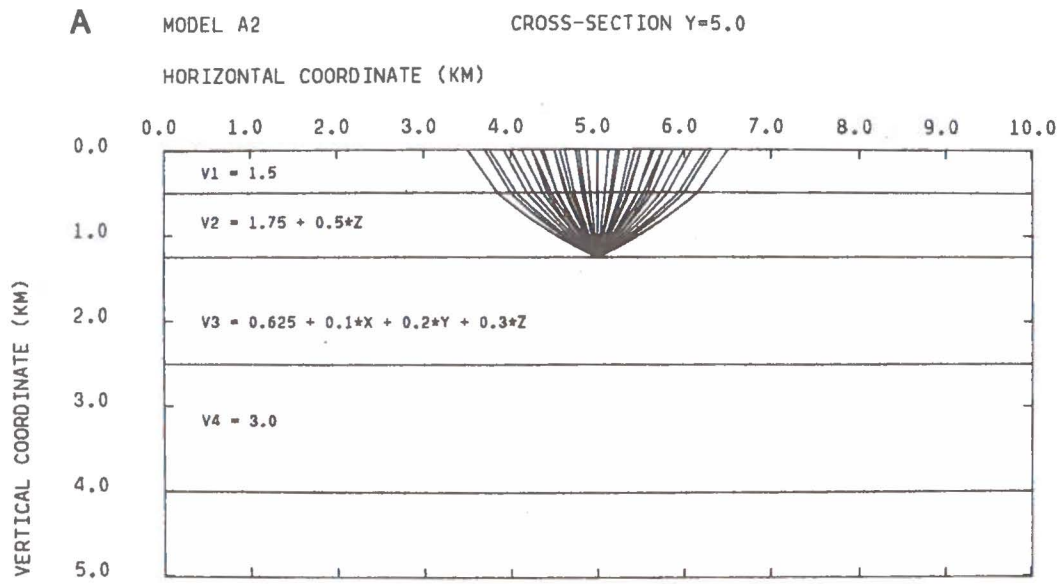


Fig.9

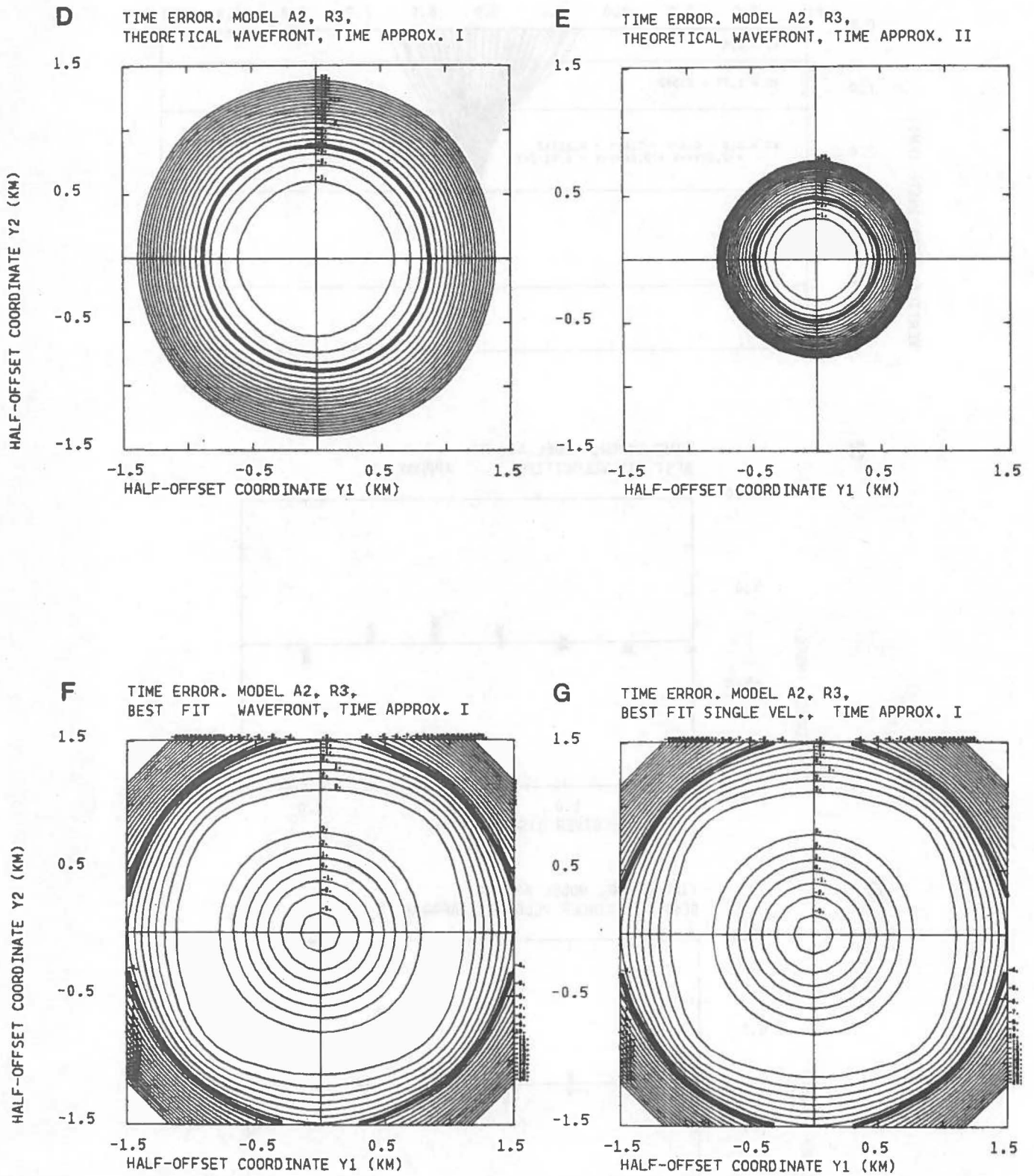


Fig.9

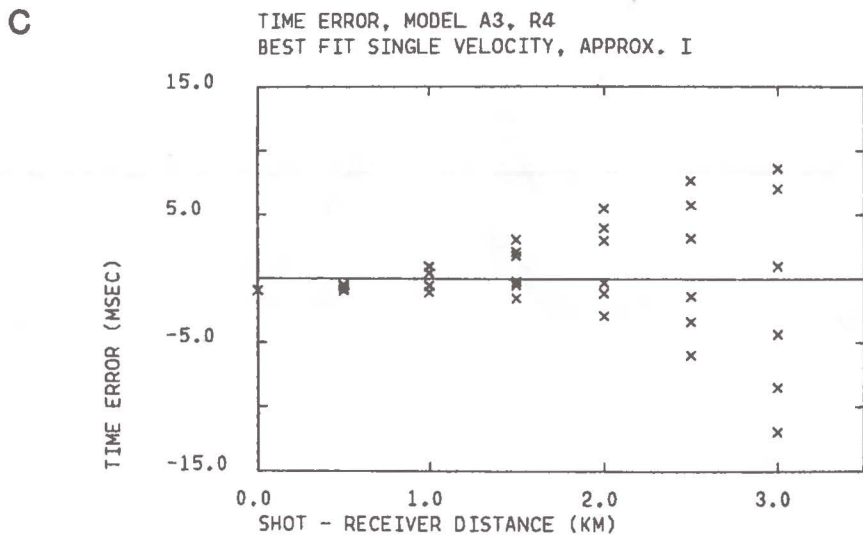
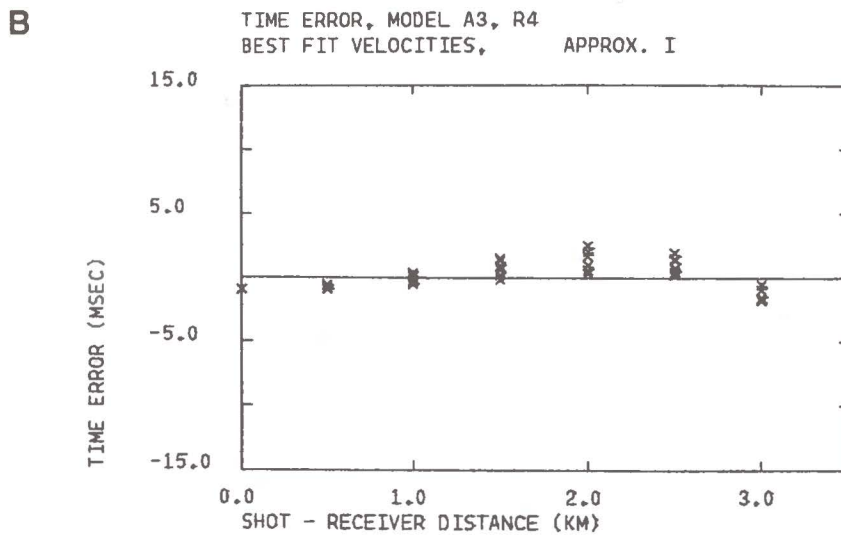
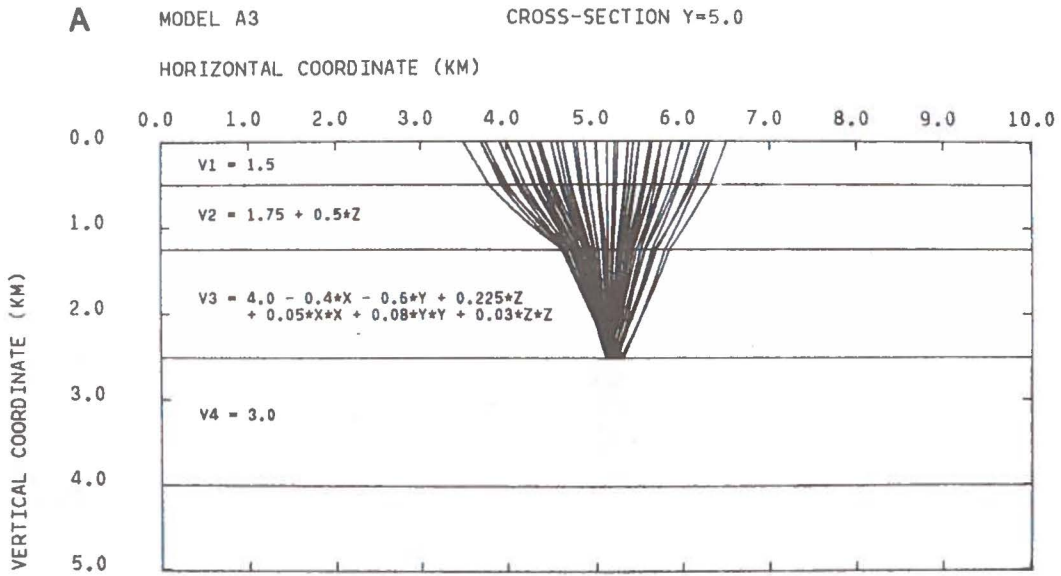


Fig.10

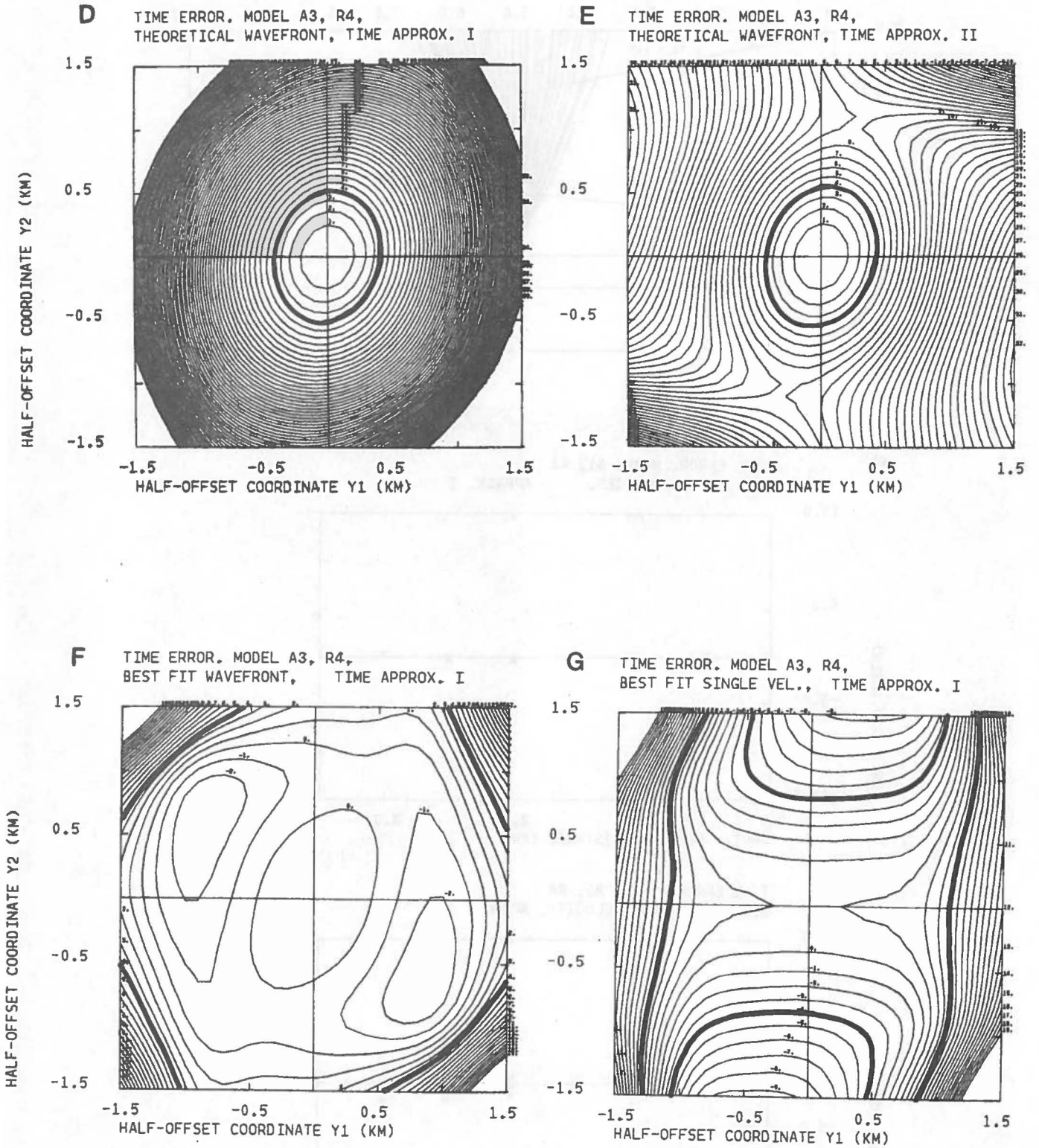


Fig. 10

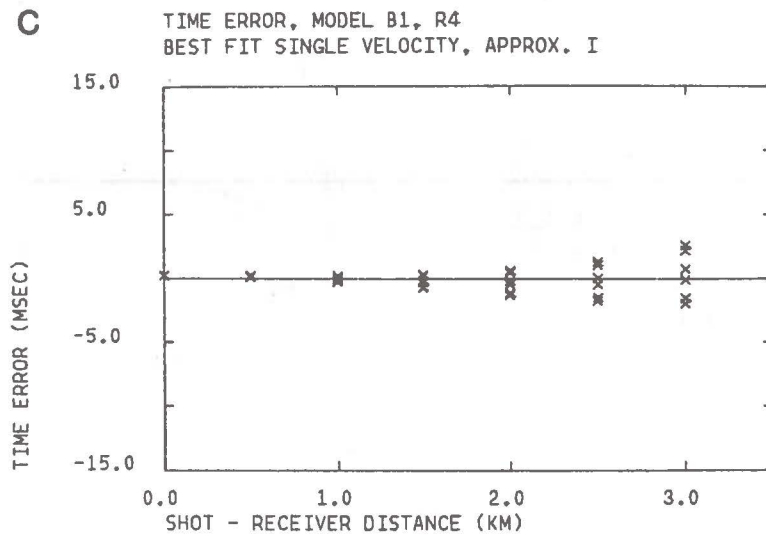
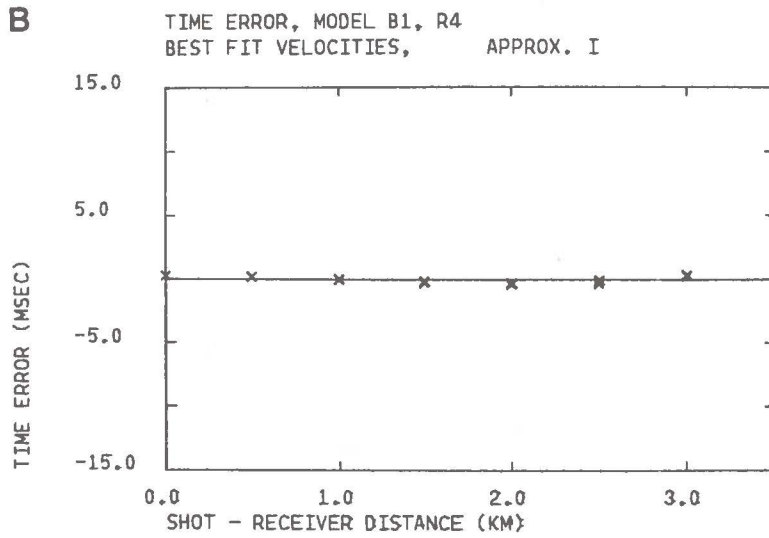
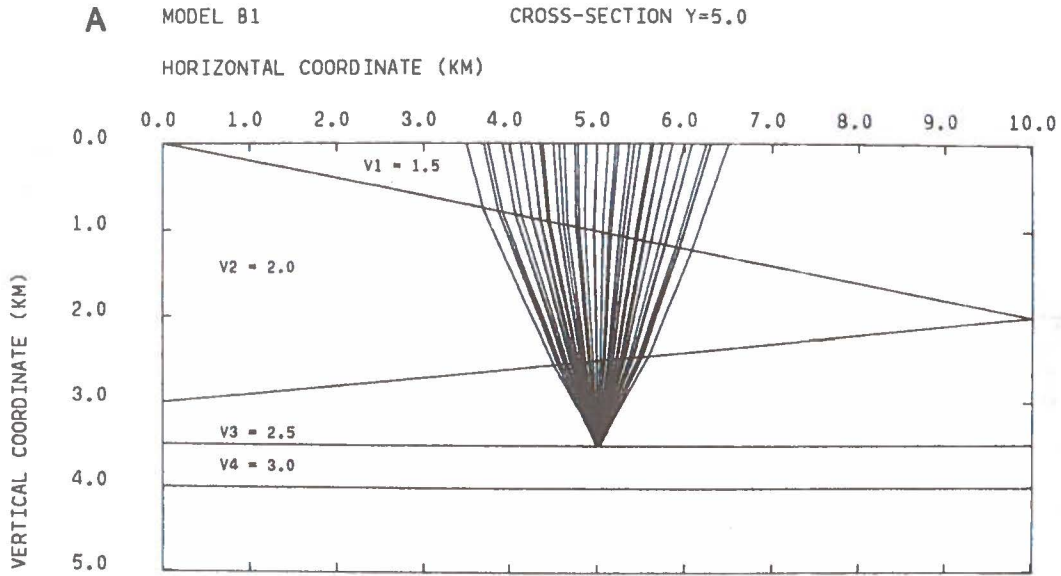


Fig. 11

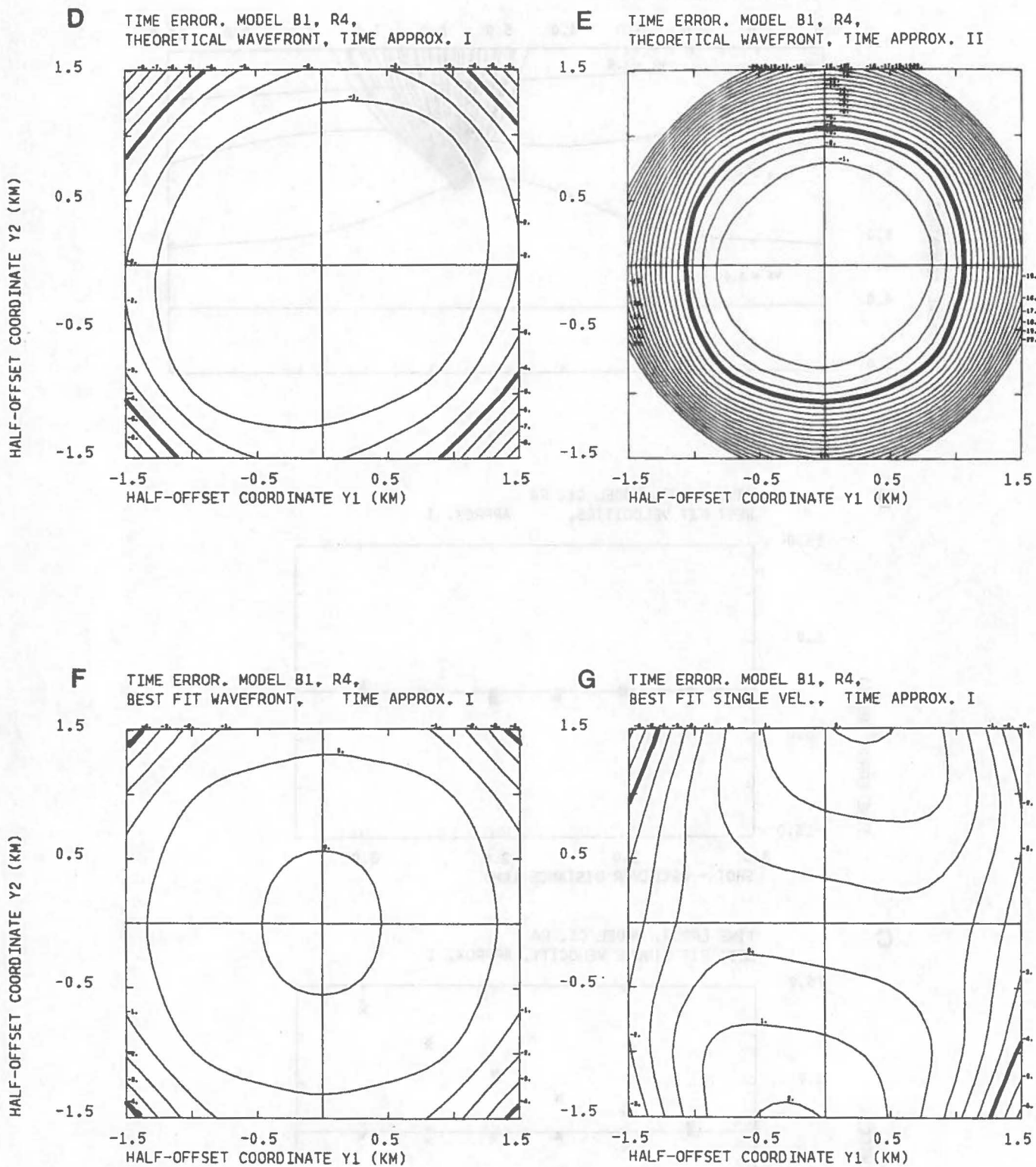


Fig. 11

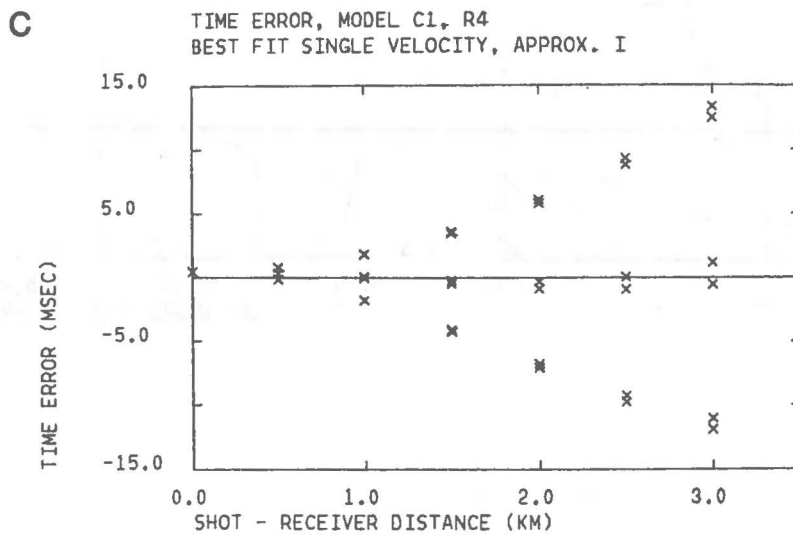
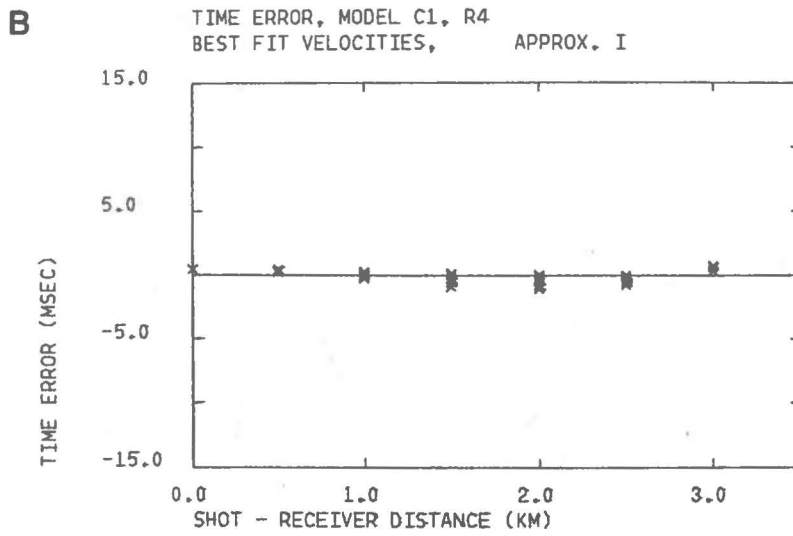
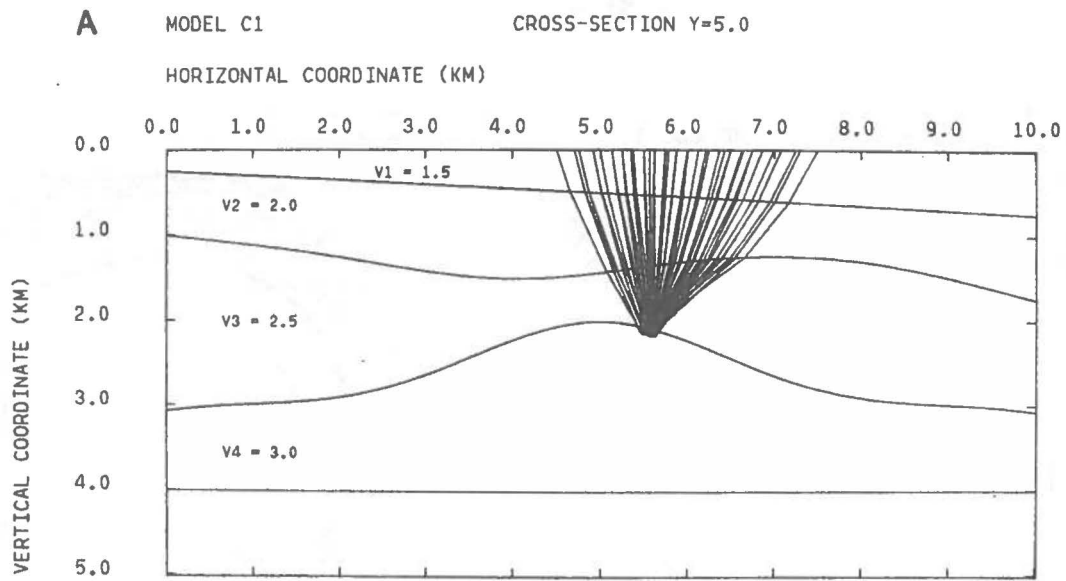


Fig. 12

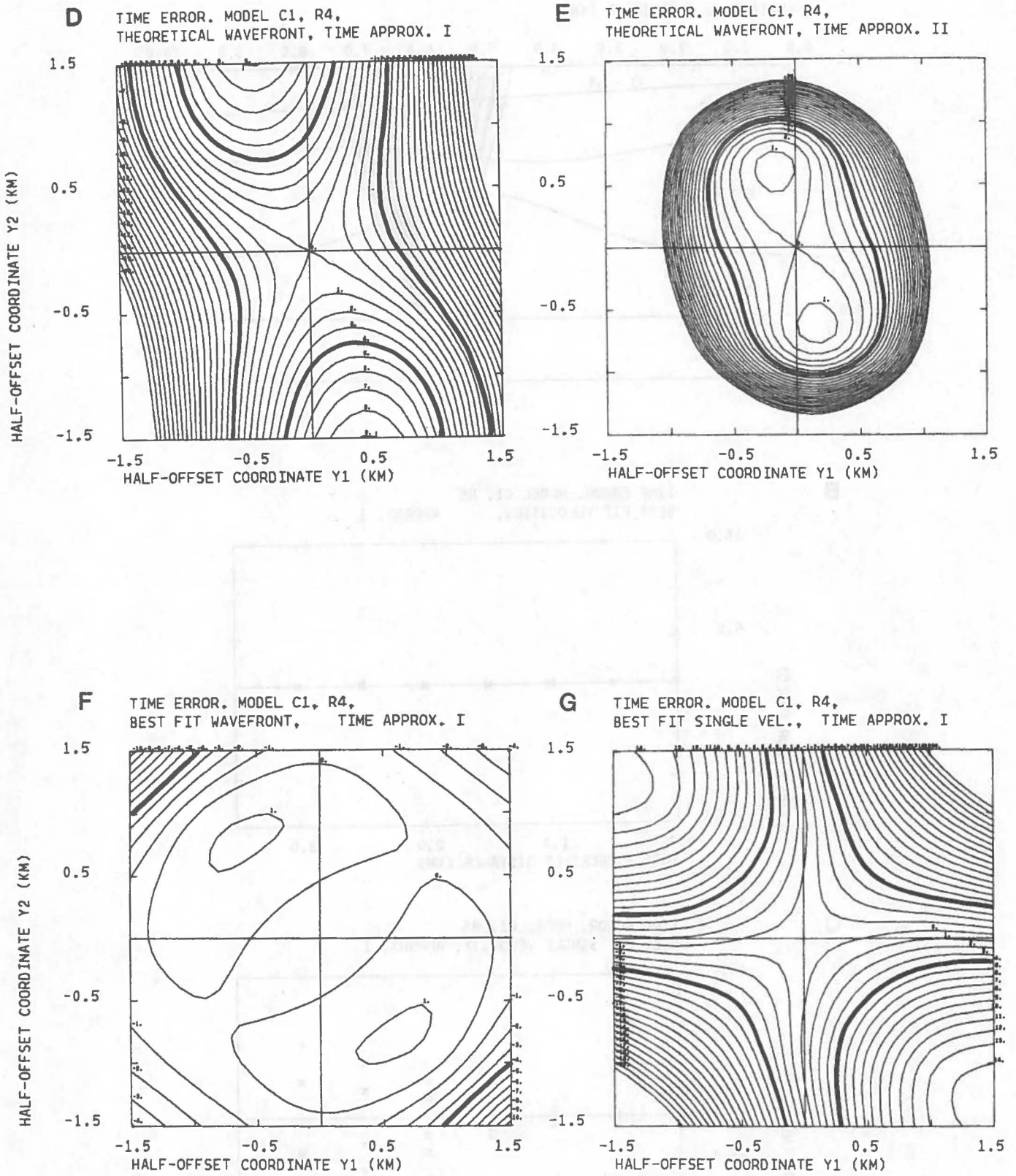


Fig.12

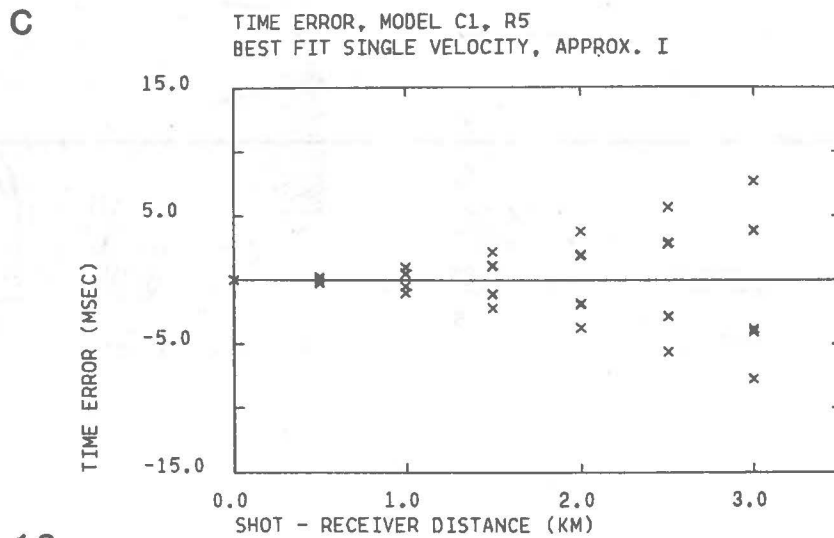
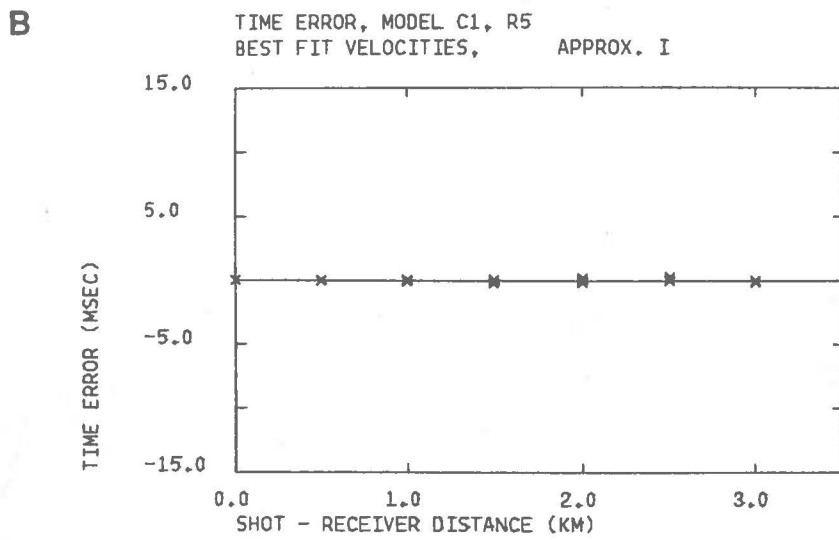
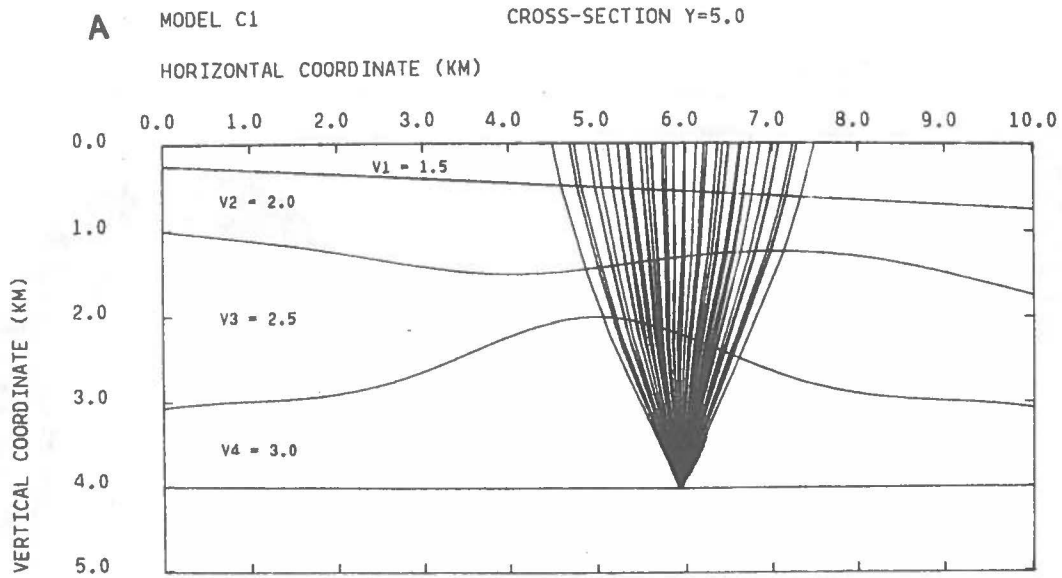


Fig. 13

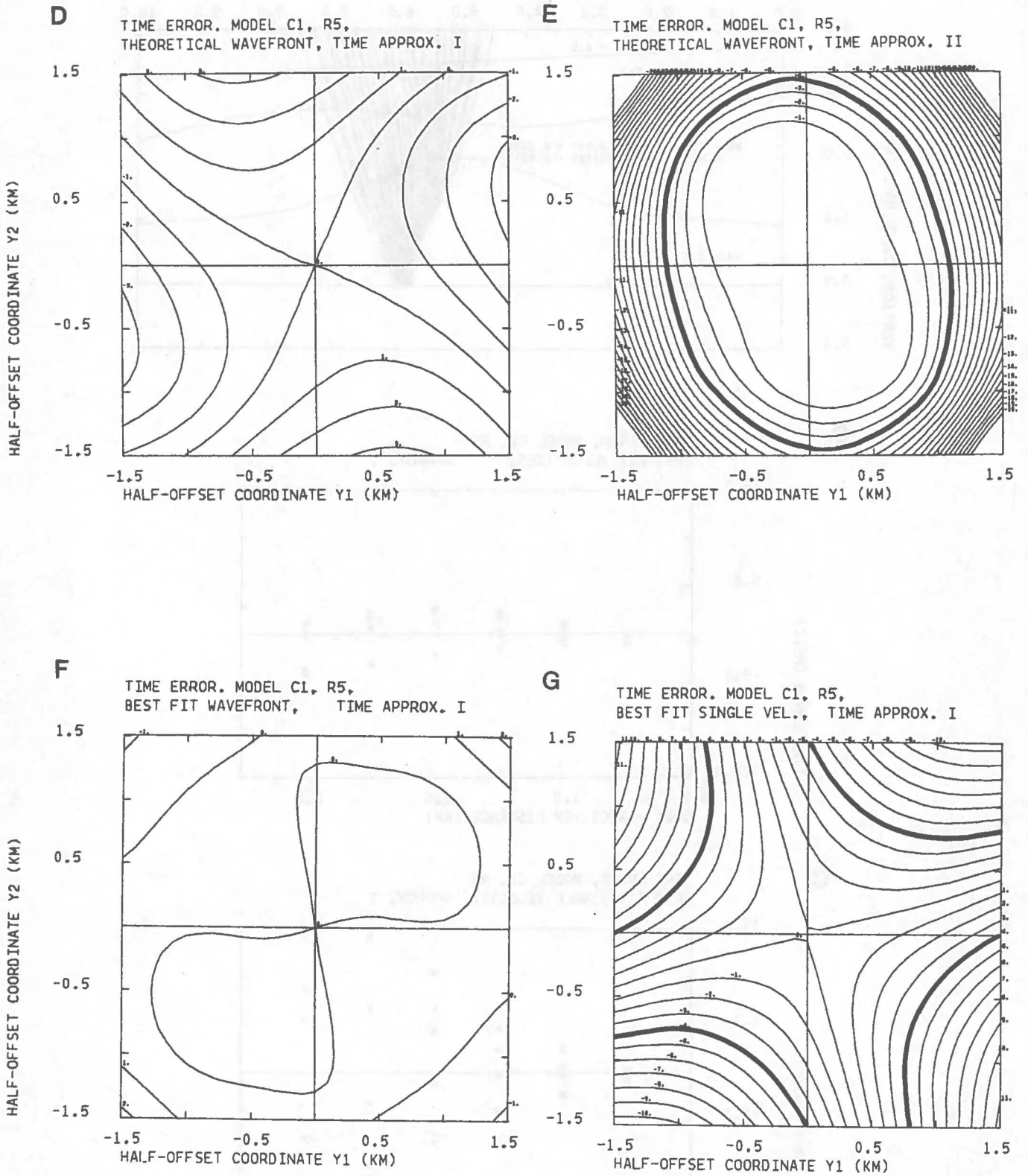


Fig. 13

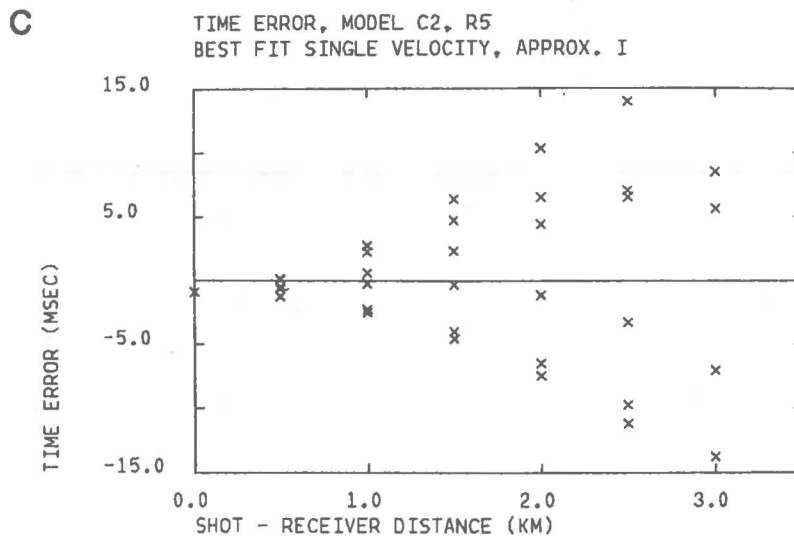
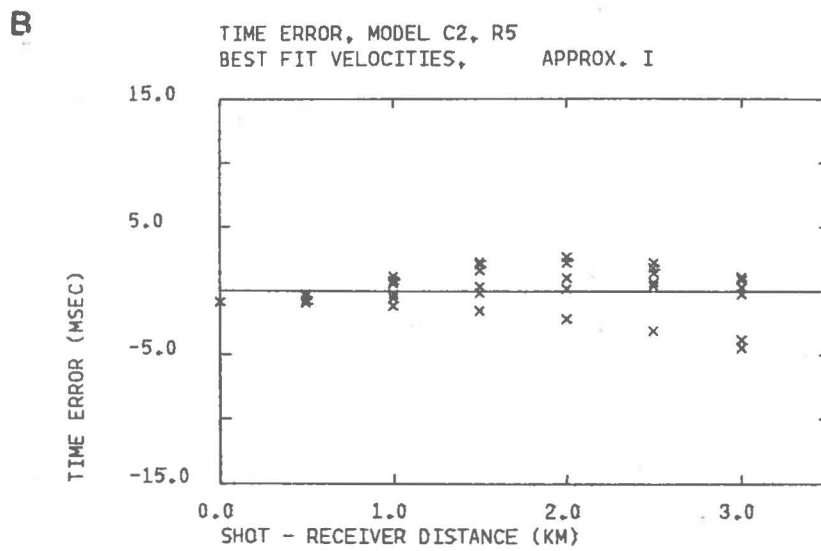
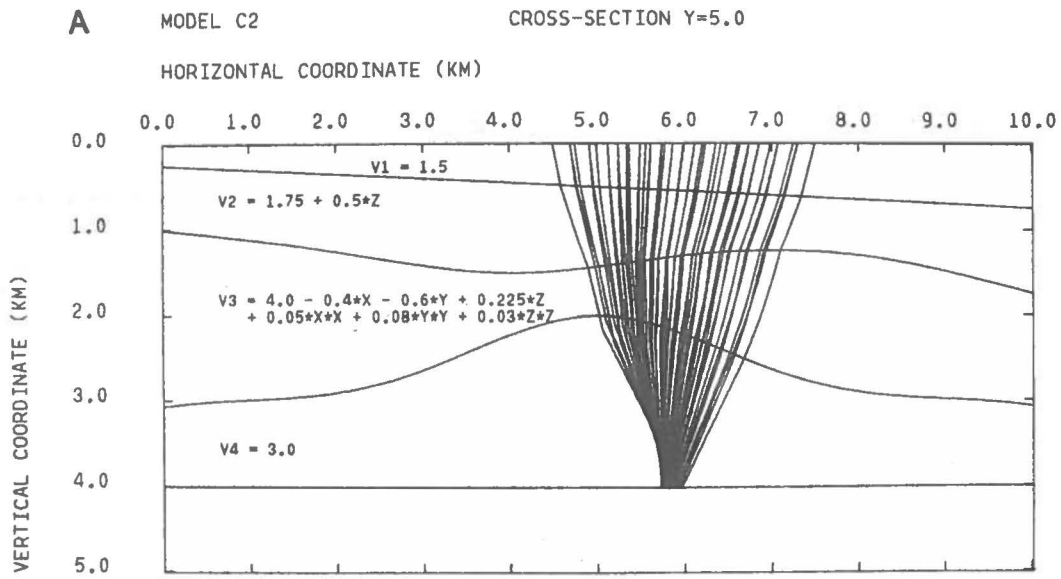


Fig. 14

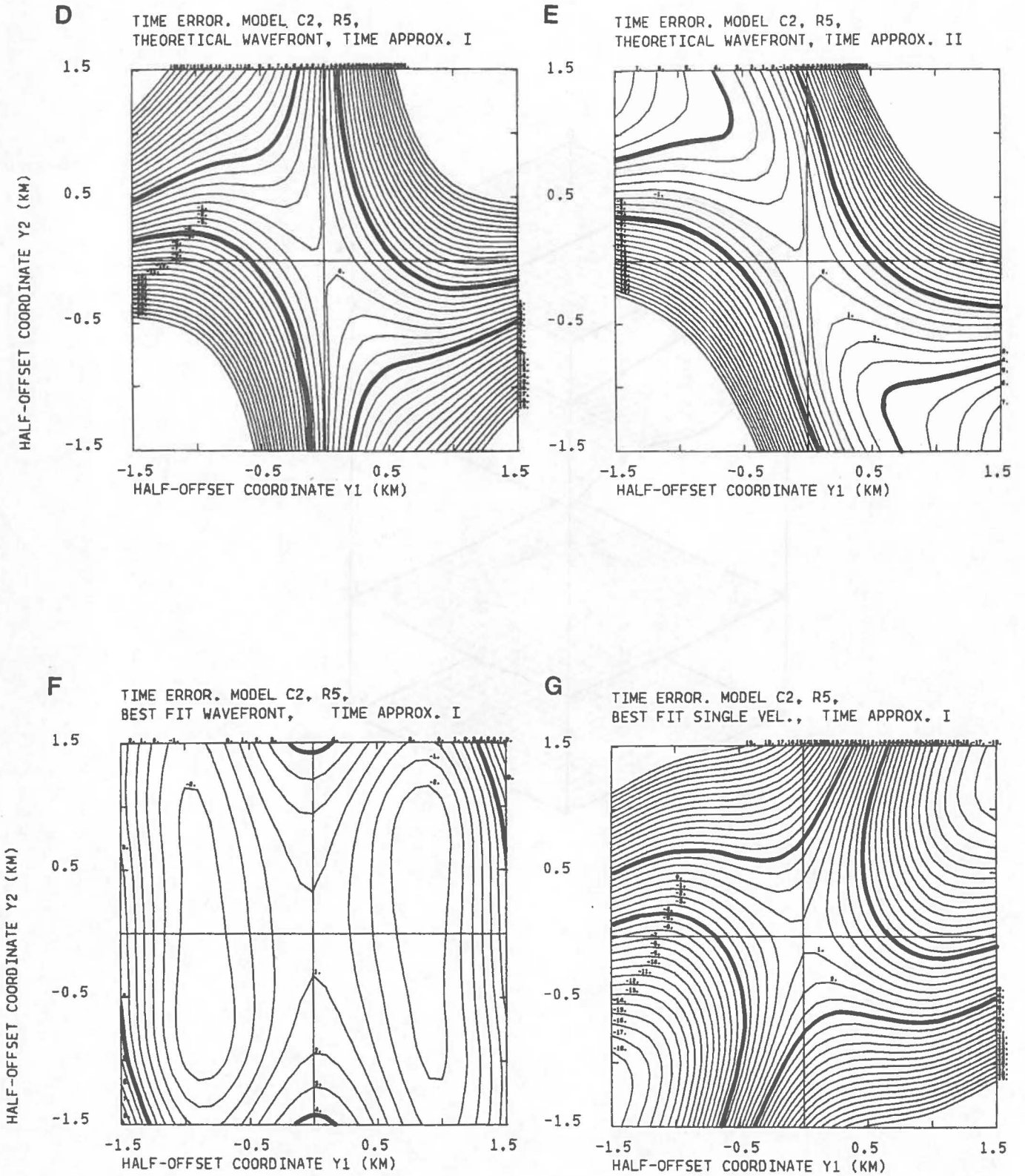


Fig. 14

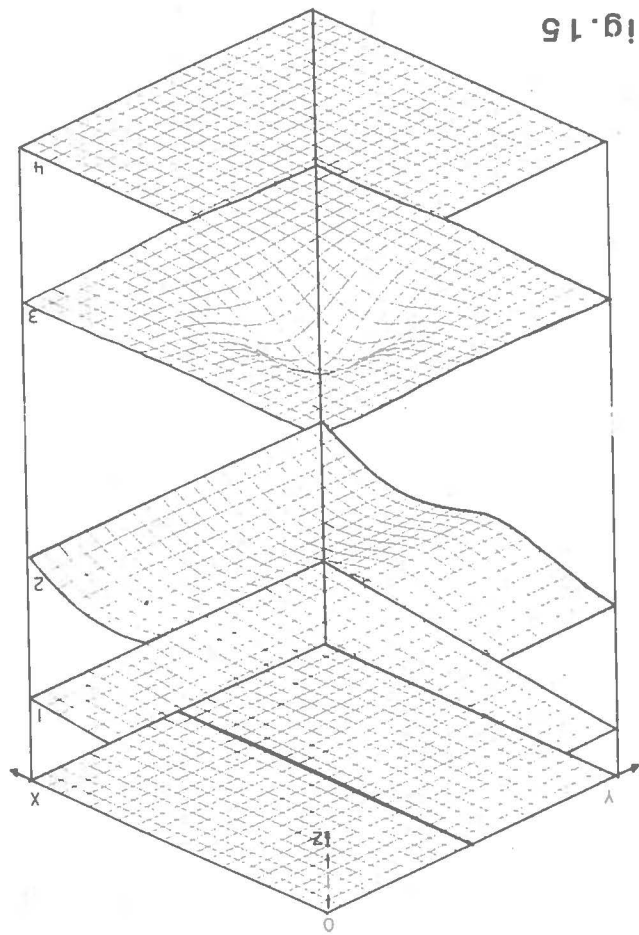


Fig. 15